Alternating Minimization Algorithm for Hybrid Precoding in Millimeter Wave MIMO Systems

Ahmed Oluwaseyi Oyedele

Submitted to the
Institute of Graduate Studies and Research
in partial fulfillment of the requirements for the degree of

Master of Science
in
Electrical and Electronic Engineering

Eastern Mediterranean University
May 2020
Gazimağusa, North Cyprus

Approval of the Institute of Graduate Studies and Research

Prof. Dr. Ali Hakan Ulusoy
Director

I certify that this thesis satisfies all the requirements as a thesis for the degree of Master of Science in Electrical and Electronic Engineering.

Assoc. Prof. Dr. Rasime Uyguroğlu
Chair, Department of Electrical and Electronic Engineering

We certify that we have read this thesis and that in our opinion it is fully adequate in scope and quality as a thesis for the degree of Master of Science in Electrical and Electronic Engineering.

Prof. Dr. Ahmet Rizaner
Co-Supervisor

Prof. Dr. Ali Hakan Ulusoy
Supervisor

Examining Committee

1. Prof. Dr. Hasan Amca

2. Prof. Dr. Ali Hakan Ulusoy

3. Assoc. Prof. Dr. Ebrahim Soujeri

ABSTRACT

Millimeter-Wave (mm-Wave) communication has been considered as the leading enabling technology for 5G networks as it provides greater spectrum other than existing cellular bands. It holds a promise to provide an unparalleled 5G cellular network capability increase. Because of the short wavelength of mm-Wave signals, Multiple-Input-Multiple-Output (MIMO) systems through precoding can exploit the use of large-scale antennas to battle rain attenuation and path loss. In contrast to the conventional MIMO systems, mm-Wave MIMO cannot perform precoding entirely at the baseband using digital precoders, as only a limited number of signal mixers and analog-to-digital converters can be supported considering their power consumption. As a cost-effective alternative, a significant attention has recently been given to a hybrid precoding transceiver architecture that combines a digital precoder with an analog precoder.

This thesis discusses an Alternating Minimization (AltMin) algorithm focused on manifold optimization for the design of a hybrid precoder, consequently comparing its results to the fully digital precoder design, that nonetheless, has a high complexity. Algorithms of AltMin are further applied to the broadband settings with orthogonal frequency division multiplexing (OFDM) modulation. Simulation results demonstrate that in terms of spectral efficiency, AltMin algorithm can significantly outperform existing algorithms and, more importantly, in some cases it can achieve an optimum performance.

Keywords: 5G, alternating minimization, hybrid precoding, low-complexity, manifold optimization, and millimeter-wave

ÖZ

Milimetre-Dalga (mm-Wave) iletişimi, mevcut hücresel bantlardan daha fazla spektrum sağladığı için 5G ağları için önemli bir olanak sağlayan teknoloji olarak düşünülmekte ve eşsiz bir 5G hücresel ağ kabiliyeti artışı sağlama vaadinde bulunmaktadır. Mm-Wave sinyallerinin kısa dalga boyu nedeniyle, Çoklu Giriş-Çoklu Çıkış (MIMO) sistemleri, ön kodlama yoluyla yol kaybı ve yağmur zayıflamasıyla savaşmak için büyük ölçekli antenlerden yararlanmaktadır. Geleneksel MIMO sistemlerinin aksine, mm-Wave MIMO, güç tüketimleri dikkate alındığında yalnızca sınırlı sayıda sinyal karıştırıcısı ve analog-dijital dönüştürücüler desteklenebildiğinden, dijital ön kodlayıcıları kullanarak ana bantta ön kodlamayı tamamen gerçekleştirememektedir. Uygun maliyetli bir alternatif olarak, dijital ön kodlayıcı ile analog ön kodlayıcıyı birleştiren hibrit bir ön kodlama alıcı-verici mimarisine son zamanlarda önem verilmektedir.

Bu tezde, hibrid ön kodlayıcıyı tasarlamak için manifold optimizasyonuna dayanan ve yüksek karmaşıklığı olan tamam dijital ön kodlayıcı performansı ile karşılaştırılabilir alternatif bir en aza indirgeme algoritması (AltMin) tartışılmaktadır. AltMin algoritmaları dikey frekans bölmeli çoğullama modülasyonu ile geniş bant ayarına genişletilebilmektedir. Benzetim sonuçları, spektral verimlilik açısından, AltMin algoritmasının mevcut algoritmalardan önemli ölçüde daha iyi performans gösterebileceğini ve daha da önemlisi bazı durumlarda optimum performansa ulaşabileceğini göstermektedir.

Anahtar Kelimeler: 5G, alternatif minimizasyon, hibrid ön kodlama, düşük karmaşıklık, manifold optimizasyonu ve milimetre dalga

DEDICATION

To my parents, my uncle and my brothers

For their love, supports, and encouragements

ACKNOWLEDGEMENTS

I would like to express my gratitude to all the people who have helped me from the day one of my MS program to its completion. I would like to thank the Almighty Allah for granting me sound health and good life thus far. I would also like to give special thanks to the best supervisor in the world, Prof. Dr. Ali Hakan Ulusoy for his outstanding patience and academic assistance. I would also like to extend my appreciation to my co-supervisor, Prof. Dr. Ahmet Rizaner for all of his academic assistance. Furthermore, I would also like to thank my parents for all of their emotional, financial and other forms of support, I won't trade them for anything in this world. I would also like to thank my brother, Professor Lukumon O. Oyedele for all of his financial support, his words of encouragement and all the good things he has done in my life. I love him beyond words can describe. I would also like to extend my gratitude to everyone in Electrical and Electronic department, all of whom include Mr. Armen Sarıca, Mustafa Mulla, Masoud and others. Lastly, I would also like to express my heartfelt gratitude to the rest of my family members (particularly my uncle, Architect Wasiu Oladipo Oyedele and his family) and friends for their encouragement and their unconditional love.

TABLE OF CONTENTS

ABSTRACT iii

ÖZ v

DEDICATION vii

ACKNOWLEDGEMENTS viii

LIST OF TABLES xi

LIST OF FIGURES xii

LIST OF SYMBOLS AND ABBREVIATIONS xiii

1 INTRODUCTION 1

1.1 Background 1

1.2 Summary of Specific Contributions 4

1.3 Motivation and Importance of Hybrid Precoding 5

1.4 Thesis Overview and Outline 6

2 LITERATURE REVIEW 8

2.1 Introduction 8

2.2 Evolution of Wireless Technology 9

2.2.1 Zero Generation Technology 9

2.2.2 First Generation Technology 10

2.2.3 Second Generation Technology 11

2.2.4 Third Generation Technology 12

2.2.5 Fourth Generation Technology 14

2.2.6 Fifth Generation Technology 14

2.3 Multiple Input Multiple Output 19

2.4 Millimeter-Wave Technology 21

2.4.1 Millimeter-Wave Free Space Propagation 22
2.5 Hybrid Precoding 24
2.6 Hybrid Precoding using Alternating Minimization Algorithms 25
3 MILLIMETER-WAVE MIMO SYSTEMS AND PRECODING 26
3.1 System Model and Problem Formulation 26
3.1.1 System Model 26
3.1.2 Channel Model 28
3.1.3 Problem Formulation 29
3.2 Hybrid Precoding focused on Manifold Optimization 30
3.2.1 Digital Baseband Precoder Design 31
3.2.2 Analog RF Precoder Design via Manifold Optimization 31
3.2.3 Hybrid Precoding Design 36
3.3 Low-Complexity Hybrid Precoding 38
3.3.1 Structure of Digital Base-band Precoders 38
3.3.2 Hybrid Precoder Design 39
3.4 Hybrid Precoding for mm-Wave MIMO-OFDM System 44
4 SIMULATION RESULTS 47
4.1 Evaluation of Spectral Efficiency 47
4.2 Low-Complexity Design 49
4.3 Hybrid Precoding for mm-Wave MIMO-OFDM Systems 52
5 CONCLUSION AND FUTURE WORK 54
REFERENCES 56

LIST OF TABLES

Table 2.1: Evolution of wireless technologies [46] 18

Table 2.2: Attenuation for different materials [55] 23

LIST OF FIGURES

Figure 1.1: Mobile data traffic volumes by application and device type 2

Figure 1.2: Evolving mobile technologies [2]. 3

Figure 1.3: A structure of hybrid precoding in mm-Wave MIMO systems where RF chain is connected to N_t and N_r antennas [56] 6

Figure 2.1: Requirements of 5G technology [43] 16

Figure 2.2: Small cell networks and the evolution of 5G [44] 16

Figure 2.3: Cellular network evolution [45] 17

Figure 2.4: Behavioral activities of MIMO system [49] 20

Figure 3.1: The tangent vector and space of a Riemannian manifold [35] 32

Figure 4.1: Spectral efficiency realized from various precoding algorithms when $N_{RF}^t = N_{RF}^r = N_s = 3$. 48

Figure 4.2: Spectral efficiency realized from various precoding algorithms where $N_s = 2$, $N_{RF}^t = N_{RF}^r = N_{RF}$ and SNR = 0 dB. 49

Figure 4.3: Spectral efficiency realized from the algorithm of MO-AltMin and PE-AltMin where $N_{RF}^t = N_{RF}^r = N_{RF} = N_s$ 50

Figure 4.4: Spectral efficiency realized from various precoding algorithms where $N_s = 6$, $N_{RF}^t = N_{RF}^r = N_{RF}$ and SNR = 0 dB. 51

Figure 4.5: Spectral efficiency obtained from various precoding algorithms in mm-Wave MIMO-OFDM systems where $N_{RF}^t = N_{RF}^r = N_{RF}$ 52

LIST OF SYMBOLS AND ABBREVIATIONS

$\|\|\boldsymbol{A}\|\|_F$	Frobenius norm of **A**
$\otimes$	Kronecker product
$\boldsymbol{A}^+$	Moore-Penrose pseudo inverse of **A**
$\boldsymbol{A}^*$	Conjugate of **A**
$\boldsymbol{A}^H$	Hermitian (Conjugate transpose) of **A**
$\boldsymbol{A}_{i,j}$	Entry on the *i*th row and *j*th column of **A**
$\boldsymbol{A}^T$	Transpose of **A**
d	Antenna spacing
det(**A**)	Determinant of **A**
E[.]	Expected part of a complex variable
F	Fourier transform
F^{-1}	Inverse Fast Fourier
$\Re[.]$	Real part of a complex variable
Tr(**A**)	Trace of **A**
Vec(**A**)	Vectorization of **A**
z^{-1}	Time delay
λ	Antenna wavelength
σ	Signal power or variance of signal
1G	First Generation
2G	Second Generation
3G	Third Generation
4G	Fourth Generation
5G	Fifth Generation Technology

AltMin	Alternating Minimization
AMPS	Advance Mobile Phone Systems
AoA	Angle of Arrival
AoD	Angle of Departure
Arg min	Argument of the minimum
BDMA	Beam Division Multiple Access
BER	Bit Error Rate
BS	Base Station
CDMA	Code Division Multiple Access
CSI	Channel State Information
EDGE	Enhanced Data rates for GSM Evolution
EHF	Extremely High Frequency
EVDO	Evolution Data Optimized
FBMC	Filter Bank Multiple Carrier
FDMA	Frequency Division Multiple Access
FFT	Fast Fourier Transform
GPRS	General Packet Radio Service
GSM	Global System for Mobile
HD	High Definition
HSDPA	High-Speed Downlink Packet Access
HSUPA	High-Speed Uplink Packet Access
IFFT	Inverse Fast Fourier Transform
IMT	International Mobile Telecommunications
IP	Internet Protocol
ISI	Inter-System Interference

ITU	International Telecommunication Union
LMMSE	Linear Minimum Mean Square Error
LTE	Long-Term Evolution
LoS	Line of Sight
MIMO	Multiple Input Multiple Output
MMB	Millimeter Mobile Broadband
MO-AltMin	Manifold Optimization based Alternating Minimization
MS	Mobile Station
MSE	Mean Square Error
NLoS	Non Line of Sight
NMT	Nordic Mobile Telephone
OFDMA	Orthogonal Frequency-Division Multiple Access
OMP	Orthogonal Matching Pursuit
PE-AltMin	Phase Extraction based Alternating Minimization
QoS	Quality of Service
SHF	Super High Frequency
SMS	Short Message Service
SNR	Signal to Noise Ratio
SOFDMA	Scalable Orthogonal Frequency-Division Multiple Access
SVD	Singular Value Decomposition
TACS	Total Access Communication System
TDMA	Time Division Multiple Access
UMTS	Universal Mobile Telecommunications Service
WCDMA	Wideband Code Division Multiple Access
Wi-Fi	Wireless Fidelity

WiMAX	World-Wide Interoperability for Microwave Access

Chapter 1

INTRODUCTION

1.1 Background

The previous century has seen the communication technologies evolved through several development and refinement. Over all, the wireless communication technology has been the fastest growing piece of the communications industry. Perhaps, it is reasonable to say that mobile and cellular communications, which directly influence our daily lives have seen the most amazing progressions of wireless communications. This has increasingly become more prominent with the shift in paradigm of communication from voice centric to data centric. The outpouring in the usage of internet, use of mobile applications, social media and online video streaming through mobile devices (mobile phones, tablets, laptops, etc.) have indicated an intense growth in the amount of data being demanded. Figure 1.1 shows the ever-increasing data requirements growth [1].

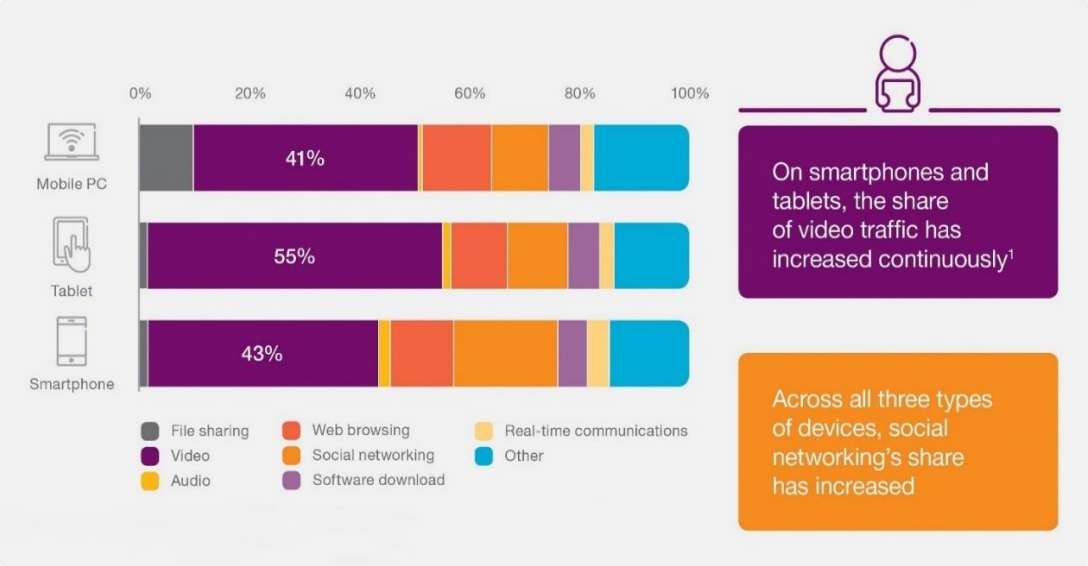

Figure 1.1: Mobile data traffic volumes by application and device type

The growth in data requirement has persistently led to an exponential demand for much higher capacity, lower latency and energy efficiency in wireless networks. Additionally, as the electromagnetic spectrum with reasonable communication properties below 20 GHz is almost entirely expended, it is apparent that the imminent demand for increased mobile data traffic capacity will be difficult to meet. These have culminated in the advancement of the Fifth Generation (5G) and beyond wireless communication systems, anticipated to be deployed by the year 2020. The 5G has key objectives of increasing the network's capacity i.e. data rates in the range of Giga (G) bits per second (bps), billions of connected devices, lower latency, and larger spectral and energy efficiencies. Other objectives include: improved coverage, reliability, and low-cost, energy efficient and environment-friendly operation. To further suggest the eminence of 5G, Figure 1.2 illustrates the evolution of mobile technologies since the advent of the First Generation (1G). While 1G established seamless mobile connectivity by introducing mobile voice services, the Second Generation (2G) increased voice capacity and delivered data to masses through mobile. The Third Generation (3G) introduced mobile broadband services for faster and better

connectivity and the Fourth Generation (4G) Long-Term Evolution (LTE) delivers more capacity for faster and better mobile broadband experience. The 5G promises to improve on the existing LTE and LTE Advanced (LTE-A) technology. Enhanced mobile broadband with faster and more reliable user experience, varied low cost Internet of Things (IoT) with a wide range of coverage, lower latency and higher reliability are a few of the design goals of 5G.

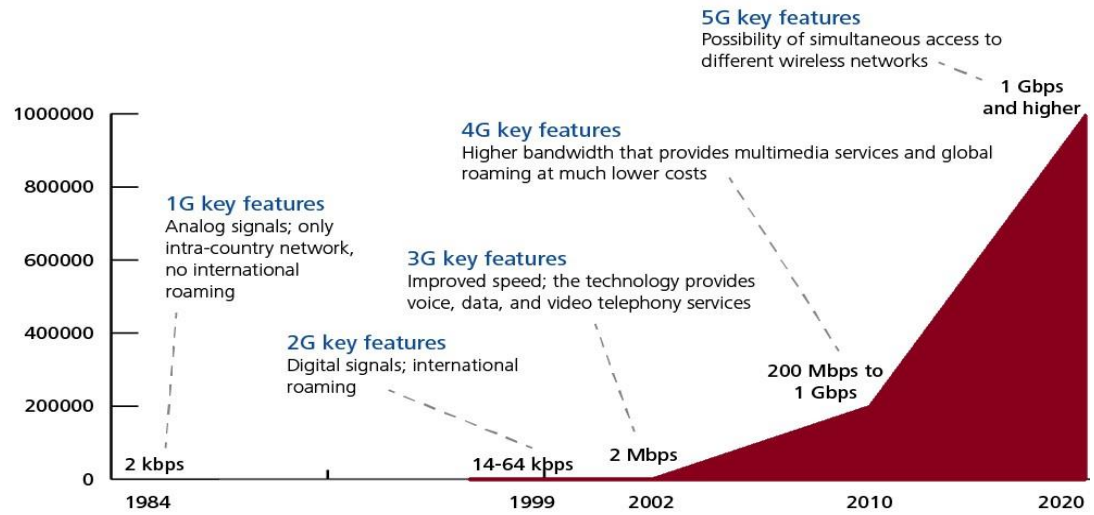

Note: Data rates based on various cellular technology generations and the years represent the deployment start.

Figure 1.2: Evolving mobile technologies [2].

Consequently, the need to improve wireless network efficiency to satisfy rising demands for high-data-rate multimedia connectivity is now dominant. A likely way to increase capacity is by improving the spectral efficiency via physical layering techniques, such as advanced channel coding and massive Multiple-Input-Multiple-Output (MIMO) [5]. Through densifying the networks, such as using small cells, and promoting cutting-edge collaboration, such as Cloud-RANs [9], [10] and enabling device-to-device communications [8] additional progress in spectral efficiency can be accomplished [6], [7]. However, the shortage of spectrum in existing cellular structures offers a fundamental impediment response to the further increase in capacity. It is

therefore important to leverage underused spectrum bands as well as those spectrum bands that are hitherto not used for cellular communications.

1.2 Summary of Specific Contributions

In this thesis, we provide an all-inclusive study of the importance of using very large antenna arrays in future wireless communications systems. Previously, millimeter-Wave (mm-Wave) bands ranging approximately between 30 GHz and 300 GHz were mostly utilized in confined and fixed points situations [3] and are now being placed headfirst as a leading candidate for a new spectral range in 5G cellular networks with a capacity of up to 10 GHz bandwidth. Recent studies in New York City have shown that outdoor cellular wireless communication is feasible for mm-Wave [4]. Initially, the core difficulties for the success of mm-Wave cellular systems are rain attenuation and massive path loss, as the carrier frequency increases in tenfold [12]. However, with the help of short wavelength of mm-Wave, mm-Wave MIMO precoding can somehow influence extensive transceiver antennas to deliver substantial beamforming gains that produce highly directional beams and battle path loss. Furthermore, by communicating several data streams by the use of spatial multiplexing, spectral efficiency can be increased further. In typical MIMO systems, digital precoders are used to carry out precoding at the baseband, which can change the phase and the magnitude of signals. On the other hand, in order to achieve a fully digital precoding, Radio Frequency (RF) chains, as well as analog-to-digital converters and signal mixers are required, similar to the number of the antenna elements. Whereas, short wavelengths of mm-Wave frequencies utilize huge amount of antenna components, the excessive usage of power by RF chains and its unaffordable cost makes digital precoding not to be feasible. Consequently, the hybrid precoding design has gained a lot of publicity with some unusual constraints in the mm-Wave MIMO framework,

which only needs a limited number of interfacing RF chains between a limited-size digital precoder and a high-size analog precoder [11]. As the analog precoders still exist to be of extraordinary dimension, implementing them via an autocratic adjustable voltage-amp in the RF domain is unrealistic [4]. The amount of phase shifters used in the designing of the hybrid precoding transceiver based on the mapping from RF chains to antennas can be shown in Figure 1.3. This fascinating structure have attracted a lot of attention and that is why this thesis studies hybrid precoding.

1.3 Motivation and Importance of Hybrid Precoding

To elaborate the significance of hybrid precoding, consider Figure 1.3 shown below, in which each of the RF chains are connected to the entire antenna element via phase shifters.

According to [11], it was noted that optimizing the spectral efficiency of mm-Wave systems could be estimated through reducing the Euclidean distance between the fully digital precoder and hybrid precoder. This reduces the architectural design of hybrid precoder as a problem of matrix factorization with its unit modulus constraints forced upon using phase shifters. Previous studies show that applying some additional constraints to analog precoder to help remove bottlenecks surrounding the analog design part using unit modulus constraints results in loss of performance. Consequently, this thesis has been inspired by reconsidering hybrid precoding strategy or, otherwise known as a problem of matrix factorization with its unit modulus constraints on analog precoder.

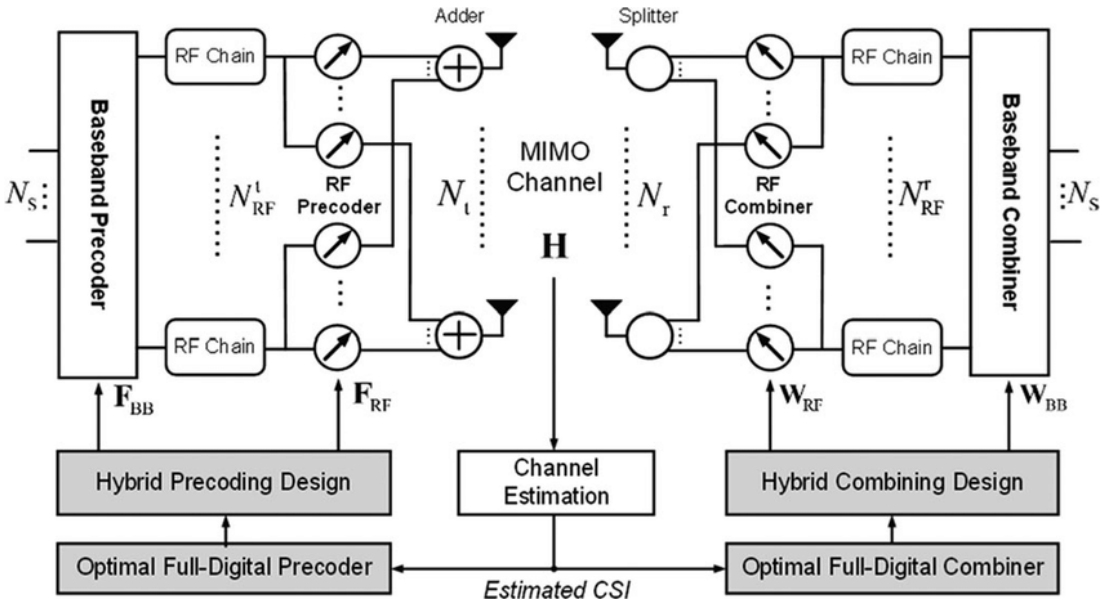

Figure 1.3: A structure of hybrid precoding in mm-Wave MIMO systems where RF chain is connected to N_t and N_r antennas [56]

1.4 Thesis Overview and Outline

This thesis focuses on Alternating Minimization (AltMin) algorithm to be the principal approach to design. This study also discusses numerous algorithms for hybrid precoding to address effectiveness of fully-optimized digital precoders. Also, grounded on that same philosophy of AltMin, this study discusses three fresh algorithms in order to effectively seek out results for hybrid precoding.

The remainder of this thesis is outlined as follows. Chapter 2 contains literature review under which evolution of wireless technology is discussed from way before 1G technology all the way up to 5G technology. Furthermore, MIMO, mm-Wave technology, hybrid precoding and AltMin algorithm for hybrid precoding are reviewed. Chapter 3 further discusses mm-Wave MIMO systems and precoding, system model, as well as channel model, and then problem formulation. Then, two AltMin algorithms are demonstrated. Lastly in this chapter, extensions of the algorithms to Orthogonal Frequency Division Multiplexing (OFDM) systems are

provided. Chapter 4 focuses on simulation results and lastly, Chapter 5 covers the concluding part of this research work together with upcoming work suggestions.

Chapter 2

LITERATURE REVIEW

2.1 Introduction

5G wireless communication networks is catching up on us and it is expected to be operational very soon. It is being power-driven by a new technology identified as mm-Wave. The mm-Wave communication is the utmost operational means of meeting the requirements of the current upsurge in internet access through wireless communication. The mm-Wave is a vastly flexible network (i.e. 5 – 20 MHz flexible channel bandwidth that reaches up to 40 MHz), and dynamic ad-hoc wireless network. This technique uses antennas that are intelligent (such as adaptive array antennas, switched beam antennas, etc.) and the flexible modulation method, that provides bidirectional high bandwidth, i.e., transfer in Gbytes, of a large volume of broadcast data over 25 Mbps connectivity and sustaining more than 60,000 connections.

However, like every novel technological breakthrough, there are unavoidable enormous initial challenges to overcome in 5G technology before it gains wide acceptance and adoption. Questions such as (how well it can go through walls, suitability over long distances and even the possibility of rain or users' hand blocking the signal) have been asked over the past few years by doubters of the technology. The impending parts will address the growth of the wireless cellular networks and certain aspects of 5G.

2.2 Evolution of Wireless Technology

In recent years, the world has witnessed an astonishing growth in the telecommunication industry especially, the wireless communication, particularly in terms of mobile technology and its user base. The mobile wireless technology began its technological development since the early 1970s, and has since gone through a series of evolutions. The technology has experienced generational technology revolution over the past few decades, namely from Zero Generation (0G) to (4G). In 1G technology, the cellular idea was launched, which made mobile wireless communication on a big scale feasible. This led to a definite change from the old fixed-telephony method to the mobile-telephony particularly since the turn of the millennium. Digital communication replaced 2G analog technology that considerably enhanced the quality of wireless communication. Furthermore, the primary emphasis of 3G systems was the convergence of emerging networks that support voice and data communication. With unrelenting research and development, 4G offers many possibilities for killer applications as well as other possible issues relating to technological advancement.

2.2.1 Zero Generation Technology

Wireless telecommunications begin with what might be called 0G. The excellent predecessor is the mobile telephone service that became accessible shortly after the second world war. During those pre cell days, the calls were set up by a network operator and only a few networks were available. 0G is referred to as a pre-cellular mobile phone technology, and an example of such were radio phones that were used in some automobiles before cellular phones were incorporated. Technologies that were utilized in 0G structures included Push to Talk, Improved Mobile Telephone Service, Mobile Telephone System, Public Land Mobile Telephony, Advanced Mobile

Telephone System, Norwegian Mobile Telephone System Offentlig, and Swedish Mobile Telephone System D or Mobile Telephone System D.

2.2.2 First Generation Technology

1G was a series of wireless protocols that was established in the 1980s and became universally known as cellular phones. The communication technology used was based on analog radio signaling. An audio communication is amplified in 1G and is distributed between two masts at a frequency greater or equal to 150 MHz. The communication process was achieved by using Frequency Division Multiple Access (FDMA). In relations to the general quality of the connection, 1G analogize poorly with its successor. It has very little capability, unstable transmission, degraded voice connections and no privacy, as audio communications would have to be replayed on radio towers, rendering these calls susceptible to undesired third-party transmission. 1G technology has maintained some advantages over 2G, though. 2G's digital signals are position and proximity dependent compared to 1G's analog signals. For instance, when 2G phone makes a call farther out from the mobile tower, the strength of the digital signal would not be powerful enough to hit it, whilst 1G phone connection lasts greater distances, but overall the strength of 1G is usually of lower quality when compared to a 2G one. This is attributable to the seamless path of the analog signal as opposed to the digital signal that has a spiky angular shape. When circumstances get worsened, the efficiency of a 1G phone call would slowly weaken, while a 2G phone call will absolutely crash. Numerous 1G specifications have been implemented in various countries. An example of such standard was Nordic Mobile Telephone that was used in Nordic countries, Russia and other Eastern Europeans. The rest are, Total Access Communications System used in the United Kingdom, United States employed the use of Advanced Mobile Phone System (AMPS), France employed RadioCom

2000 (RC2000), West Germany used Radio Telephone Network C (C-Netz), while Italy used Radio Telefono Mobile Integrato (RTMI).

2.2.3 Second Generation Technology

In 2G, information like applications and email cannot be transferred, except making phone calls, as well as fundamental supplementary details like date and time. However, SMS messages for some norms is regarded as a type of data transmission. Radiolinja (now part of Elisa Oyj) launched 2G cellular telecommunication network for commercial purpose on the Finnish Global System for Mobile (GSM) communication customary in 1991. 2G strategies can be classified in Time Division Multiple Access (TDMA) and Code Division Multiple Access (CDMA) based principles which is dependent on the multiplexing used. 2G uses a compression decompression algorithm for digital voice information compression and multiplex. Typically, 2G cellular phones are smaller in size compared to 1G, because they had minimal radio power. One of the advantages of 2G have been that digital signals requires less energy consumption, thus helping phone batteries last longer. Digital coding makes voice more audible and decreases noise. Another benefit of 2G is that it supports for protection and confidentiality of voice and data through digital encryption.

In spite of the achievement accomplished in 2G, the term General Packet Radio Service (GPRS) also known as second and a half generation (2.5G) was later introduced, a cellular wireless technology used to define 2G-systems that have implemented a packet switched domain in addition to the circuit switched domain. GPRS can possibly provide data rates starting from 56 kbps up to 115 kbps. It can offer services such as wireless application protocol access, multimedia messaging service, internet communication services such as emails, world wide web access, mobile games, search and directory.

Another further wireless technological improvement to 2G systems was 2.75G often referred to as Enhanced Data rates for GSM Evolution (EDGE). EDGE technology is an improved GSM variant, which allows data and information more transparent and easier to relay. Due to its versatility, EDGE technology is favored over GSM because of its ability to convey packet transfer and circuit transfer data. In contrast to GPRS technology it often moves data more quickly. An illustration is a standard text file which would usually take 6 seconds to be transferred in GPRS but requires just 2 seconds in EDGE.

2.2.4 Third Generation Technology

3G technology is based on the International Telecommunication Union family of standards under the International Mobile Telecommunications platform, IMT-2000. 3G technologies offer improved network capacity through improved spectral efficiency and offer services which include wide area wireless voice telephony, video calls and broadband wireless data, all within a mobile setting. Other features include high-speed packet access data transmission capabilities competent to deliver speeds up to 14.4 Mbps on the downlink and 5.8 Mbps on the uplink. 3G technologies make use of TDMA and CDMA. The fundamental characteristics of 3G technology is fast data transfer rates. 3G technology is highly versatile because it is capable of supporting 5 main radio systems. These radio systems work under FDMA, TDMA, and CDMA. While FDMA has only one radio interface or frequency code, TDMA accounts for time code, and single carrier and CDMA holds for direct spread, and multi carrier.

To further help improve 3G technology, the term third and a half generation (3.5G) known as High-Speed Downlink Packet Access (HSDPA) was introduced. A telephony protocol that provides an innovative path for Universal Mobile Telecommunication Systems (UMTS) based 3G networks allowing for higher data

transfer speeds. HSDPA has a data transmission rate of up to 8-10 Mbps and 20 Mbps for MIMO systems over a 5 MHz bandwidth in Wideband CDMA (WCDMA) downlink. Another technology introduced in 3.5G is Evolution Data Optimized (EVDO). EVDO is a technological innovation for delivering fast internet access via mobile broadband adapters and WLANs in CDMA-based mobile carriers. In terms of download speed, up to 14.7 Mbps can be supported by EVDO, and up to a limit of 5.4 Mbps can be used for streaming. It provides data-only capabilities and utilizes a dedicated 1.25 MHz channel when installed.

Another further wireless hi-tech improvement to 3G and 3.5G technologies was 3.75G known as High-Speed Uplink Packet Access (HSUPA). The essence of this technology is to compliment HSDPA and to also provide better coverage area. Initially, HSUPA increases uplink UMTS / WCDMA to 1.4 Mbps and later up to 5.8 Mbps. HSUPA enables specialized user technologies at larger and symmetrical data speeds, such as instant email and online person to person game play in real time. In that regard, Orthogonal Frequency-Division Multiple Access (OFDMA) was introduced and is a key feature of the IEEE Wi-Fi 6 (802.11ax) standard, that enables access points to be used concurrently by many clients thereby, eliminating the need for router to wait for medium connectivity on each packet. Other innovations include Scalable OFDMA (SOFDMA) and Fixed WiMAX. SOFDMA brings scalability to OFDMA by reducing smaller channel system complexities and increasing wider channel efficiency. Fixed WiMAX on the other hand belongs to a technology that is designed using IEEE 802.16-2004 (802.16d) standard that utilizes OFDM as the air interface. When deployed, they are not ideal for handoffs among base stations therefore, the services providers cannot provide mobility.

2.2.5 Fourth Generation Technology

4G refers to all Internet Protocol (IP) packet switched networks, mobile ultra-broadband (gigabit speed) access and multi-carrier transmission. Its commercial wireless network was first publicly launched in 2010. 4G effectively expands 3G infrastructure with greater bandwidth and offers all the services in 3G networks. 4G infrastructure has an outstanding audio / video connectivity through end-to-end IPs. Since the advent of 4G communications, some companies have pegged wireless devices to a 100 Mbps and up to 1 Gbps for local area connectivity. High-Definition (HD) TV quality and HD video-conference facilities have been made realizable as well as game-streaming services by 4G technologies. The term “MAGIC” often applies to 4G wireless technology that stands for Mobile Multimedia, Anywhere, Global Mobility Solutions, Integrated Wireless and Customized Services. Hence, Mobile WiMAX was brought to light. It conforms to IEEE 802.16e-2005 and it is capable of transmitting a wireless link from one base station to another as the user travels, without having to drop the link.

2.2.6 Fifth Generation Technology

5G denotes the next phase of mobile telecommunication requirements. With 5G technology, the telecom industry will experience a modern technological transition. In addition to speed enhancement, 5G is expected to unlock a massive IoT environment, where networks will support millions and millions of mobile devices with the right balance of speed, latency and cost. In helping to cope with system capacity and handling of huge number of clients, technologies like Beam Division Multiple Access (BDMA) could be used. In fact, engineers from Korea have proposed BDMA as a radio protocol for 5G system because of its independency from time and frequency infrastructure. BDMA does not only solve the bandwidth and efficiency problem, but

also reduces signal degradation at the edge of the cell. Other valuable technologies that have also demonstrated their capabilities in providing better and quality communications in 5G includes Filter Bank Multiple Carrier (FBMC). It handles the drawbacks of OFDM by providing high efficiency bandwidth. Furthermore, in keeping with the rules of communication, the smaller the frequency, the bigger the bandwidths, thus, using smaller frequencies for 5G networks (mm-Waves between 30 GHz and 300 GHz) is why 5G can be a lot quicker. Furthermore, 5G technology provides extremely low latency rate, the delay between sending and receiving of information. From 200 milliseconds (ms) for 4G, to 1 ms with 5G. Envision a world where a vehicle reacts 250 times quicker than you. Visualize a scenario where it could respond to thousands of incoming data and transmit its reactions back in 1 ms to other cars and road signals. For example, the reaction distance at 100 kilometers per hour (km/h) is about 30 meters before the brakes are pulled. Using a response time of 1 ms, the vehicle would only have rolled less than 3 centimeters. Figure 2.1 explains ultimately how 5G technology is driven by the following 8 specification requirements:

- Up to 10 Gbps data rate (10 to 100x improvement over 4G networks)
- 1 ms point to point latency
- 1000x bandwidth per unit area
- Up to 100x number of connected devices (compared to 4G LTE) per unit area
- 99.999% availability
- 100% coverage
- 90% reduction in network energy usage
- Up to 10-year battery life for low power IoT device

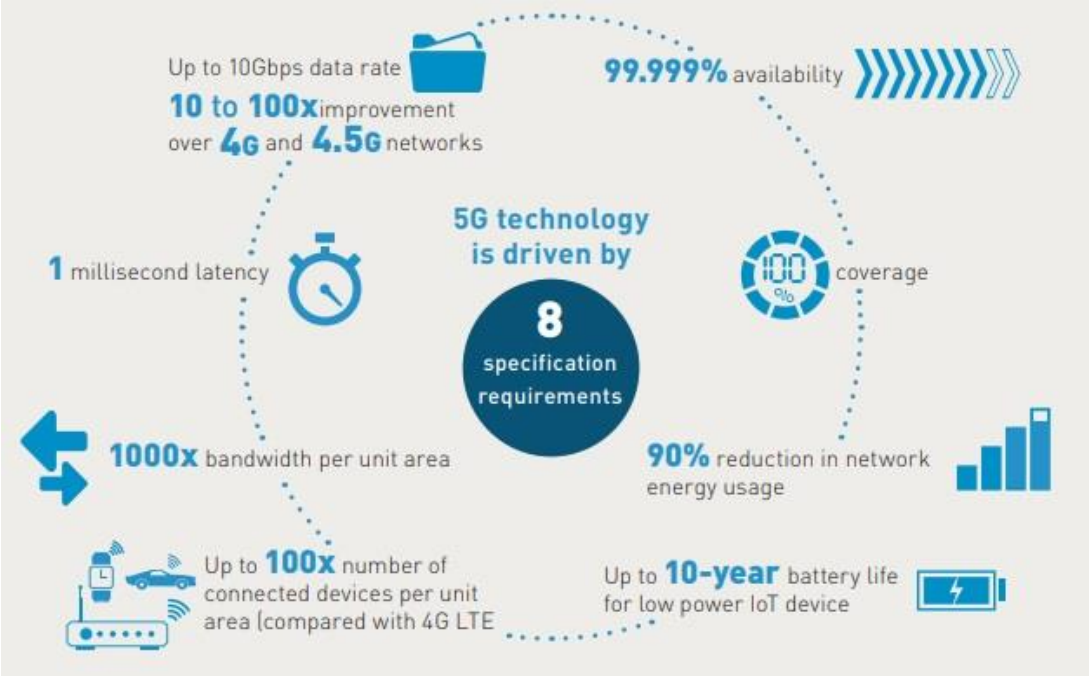

Figure 2.1: Requirements of 5G technology [43]

Figure 2.2 shows wireless infrastructure of 5G and how small cells fit into the evolution of 5G.

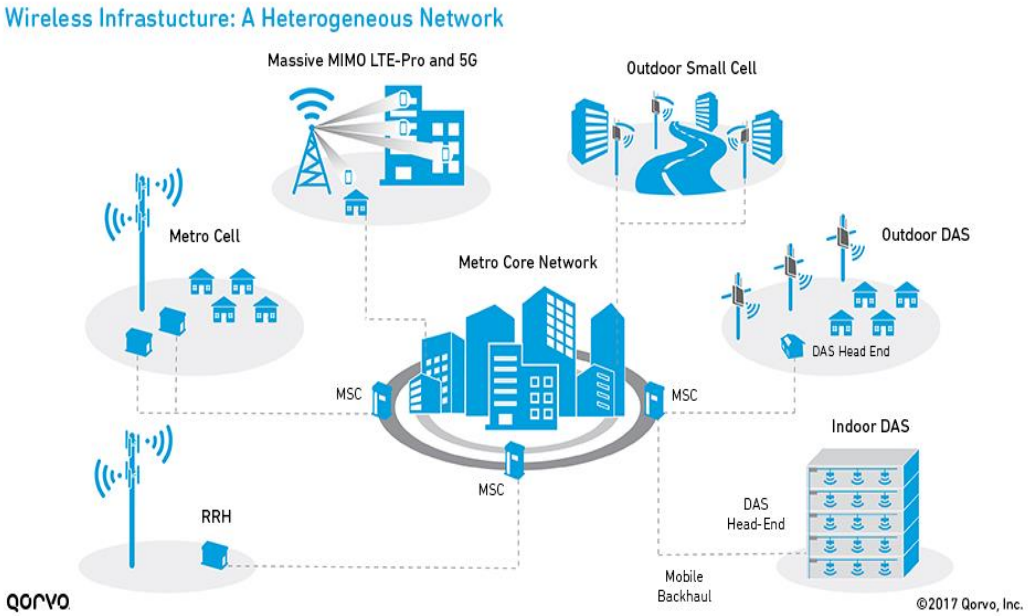

Figure 2.2: Small cell networks and the evolution of 5G [44]

Sequel to all the generations discussed from 0G to 5G, the last four decades of evolution of the cellular network have seen not only an increase in speed, but also an increasing demand for onboard memory in devices. Figure 2.3 shows the evolution of wireless cellular network.

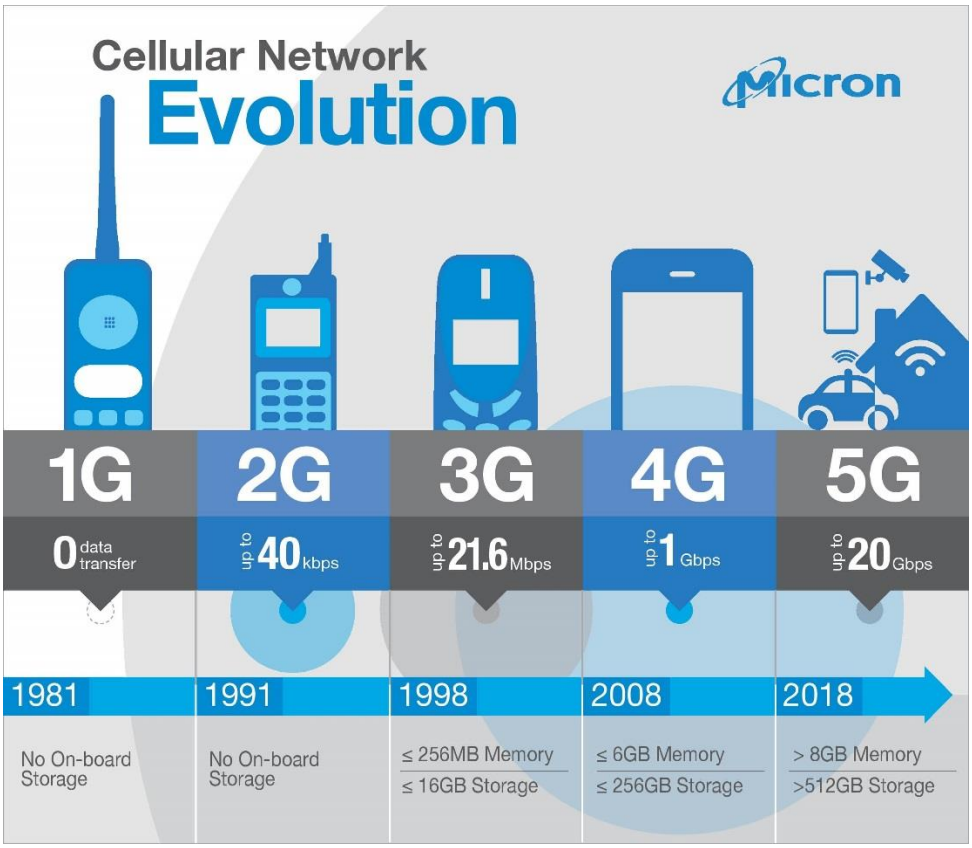

Figure 2.3: Cellular network evolution [45]

Table 2.1 further shows the comparison among the entire generations of wireless communication systems and their capabilities. Also, it reveals the general purpose of a 5G wireless data technology.

Table 2.1: Evolution of wireless technologies [46]

Generation	Access Technology	Bandwidth	Frequency Band	Data Rate	Forward Error Correction	Application
1G	AMPS, FDMA	30 KHz	800 MHz	2.4 Kbps	-	Voice
2G	CDMA	1.25 MHz	850/900/1800 /1900 MHz	10 Kbps	-	Voice and data
	GSM, TDMA	200 KHz				
2.5G	GPRS			50 Kbps		
2.75G	EDGE			200 Kbps		
3G	UMTS, WCDMA	5 MHz	800/850/1800 /1900/2100 MHz	384 Kbps	Turbo codes	Data service, voice and video calling
	CDMA2000	1.25 MHz				
3.5G	HSUPA / HSDPA	5 MHz		30 Mbps		
	EVDO	1.25 MHz				
3.75G	LTE, OFDMA) / Single Carrier FDMA (SC-FDMA)	20 MHz	1.8-2.6 GHz	200 Mbps	Concatenated codes	HD TV and online gaming
	SOFDMA, Fixed WiMAX	7-10 MHz	3.5-5.8 GHz			
4G	LTE-A, OFDMA/SC-FDMA	20 MHz	1.8-2.6 GHz	DL: 3 Gbps UL: 1.5 Gbps	Turbo codes	HD TV and online gaming
	SOFDMA, Mobile WiMAX	3.5-8.75 MHz	2.3-2.5 GHz	200 Mbps		
5G	BDMA, FBMC	60 GHz	1.8-300 GHz	50 Gbps	Low density parity check code	Ultra-HD video and virtual reality

2.3 Multiple Input Multiple Output

In a MIMO communication system, there is a Transmitter (T_X) that conveys data through multiple transmitting antennas and a Receiver (R_X) that accepts data through multiple receiving antennas. It should be noted that in general the number of antennas at the transmitter N_t indicates the degree of freedom and the number of antennas at the receiver N_r indicates the diversity order of the MIMO networks. The binary data to be transmitted is often distributed between the transmitting antennas and each receiving antenna collects data from all the transmitting antennas, hence, if there are N_t transmitting antennas and N_r receiving antennas, at that point, the signal will propagate over $N_t \times N_r$ channels, with each channel having its own response.

MIMO wireless communication systems are convenient in a way that they make it possible to increase the efficiency of the wireless connection between the transmitter and the receiver compared to previous systems in order to obtain higher data rates. The rich multi-path environment enables many orthogonal channels to be created between the transmitter and the receiver. Moreover, using the same bandwidth, data can then be distributed over the air in parallel, over those channels simultaneously. As a result, higher spectral efficiencies are achieved compared to non-MIMO systems. Figure 2.4 demonstrates the behavioral activities of a MIMO system.

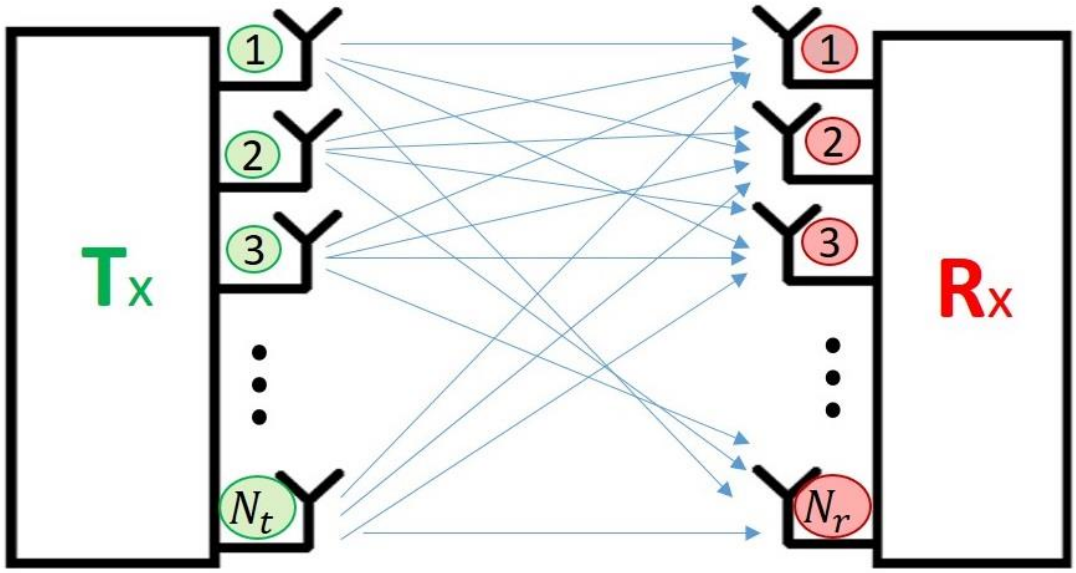

Figure 2.4: Behavioral activities of MIMO system [49]

MIMO systems can be expressed as:

$$\mathbf{y} = \mathbf{Hx} + \mathbf{n} \tag{2.1}$$

where $\mathbf{y} = [\, y_1 y_2 \cdots y_{N_t}]^T$ is a vector of communication signals received at a receiver;

$\mathbf{x} = [\, x_1 x_2 \cdots x_{N_r}]^T$ is a vector of communication signals transmitted by a transmitter;

$\mathbf{n} = [\, n_1 n_2 \cdots n_N]^T$ is a vector of noise components affecting the transmitted signals;

$\mathbf{H} = \begin{bmatrix} h_{1,1} & \cdots & h_{1,N_r} \\ \vdots & \ddots & \vdots \\ h_{N_t,1} & \cdots & h_{N_t,N_r} \end{bmatrix}$ is a channel matrix of communication channel attenuation factors;

N_r is the number of antennas at the receiver and

N_t is the number of antennas at the transmitter.

Therefore (2.2) displays the signal pattern obtained for a MIMO device,

$$\begin{bmatrix} y_1 \\ \vdots \\ y_{N_t} \end{bmatrix} = \begin{bmatrix} h_{1,1} & \cdots & h_{1,N_r} \\ \vdots & \ddots & \vdots \\ h_{N_t,1} & \cdots & h_{N_t,N_r} \end{bmatrix} \begin{bmatrix} x_1 \\ \vdots \\ x_{N_r} \end{bmatrix} + \begin{bmatrix} n_1 \\ \vdots \\ n_{N_t} \end{bmatrix} \quad (2.2)$$

MIMO systems take advantage of the spatial diversity that is acquired through spatially separated antennas in a dense multipath scattering setting and can be implemented in numerous ways to either acquire a diversity gain to combat signal fading or to obtain capacity gain. It is worthy of note that diversity technique is a popular approach to combat fading, interference from co-channel and error outburst. Techniques of diversity can be used at both base stations and mobile receptors. The diversity combining technique however is an important technique in communication systems that is applied on the received signal. It is classified into three basic techniques: selection diversity, equal gain combining, and maximum ratio combining. Furthermore, MIMO system generally has three categories of technique, first of all, it aims at boosting energy output by optimizing spatial diversity, which includes diversity in delays, codes for space-time block [50], [51] and codes for space-time trellis [52]. The second goal utilizes a more layered technological strategy for capacity building. A common example is the V-BLAST method, which usually does not have maximum spatial diversity [53]. Ultimately, the third form uses the information of the channel on the transmitter by decomposing the coefficient matrix of the channel with the aid of a Single Value Decomposition (SVD) and utilizes such unitary decomposite matrices as a preset and a post filter for the transmitter and receiver to accomplish a capacity that is nearly full [54].

2.4 Millimeter-Wave Technology

The production and popularity of smartphones and other mobile data devices such as netbooks and eBook readers have led to an extraordinary growth in the mobile data traffic. According to experts, with more than a thousand-fold increase over the next 10

years, the mobile data usage will grow at a compound annual growth rate of 108%. Thus, improvements in air interface capability and new spectrum allocation are of great importance in terms of achieving this exponential rise [47]. Therefore, the spectrum in the 30-300 GHz has often been labeled an exceptionally high frequency or mm-Wave band. With wavelengths ranging from 1 to 100 mm has ignited the interest of many in the mobile communication industry and is currently being exploited in 5G technology. For point-to-point communication, there are already mm-Wave communication systems that can reach multi-gigabit data rates at a range of up to a few kilometers. Yet, the electronic components used includes power amplifiers, low-noise amplifiers, mixers, and antennas, are too large in size and consume immense power to be applicable in mobile communication. Furthermore, mm-Waves are absorbed in the atmosphere by oxygen and water vapor. As the oxygen molecule is absorbing electromagnetic energy at around 60 GHz, attenuations of around 15 dB/km can occur within the 57-64 GHz oxygen absorption band. As for water vapor absorption rate, it depends on the volume of water vapor and can reach tens of dBs in the range between 164 and 200 GHz [48]. We therefore disregard these bands because the propagation spectrum for mobile broadband applications in those bands would be limited. Nevertheless, with a realistic hypothesis that over time 40 percent of the current spectrum will be made available, mm-Wave Mobile Broadband (MMB) unlocks the path to a prospective new 100 GHz digital wireless networking spectrum.

2.4.1 Millimeter-Wave Free Space Propagation

The loss of mm-Wave transmission is largely due to free space loss. Some wireless engineers misunderstand that loss of free space distribution is depending on frequency, and that lower frequencies are better propagated when compared to higher frequencies. The indicated confusion can be referenced to radio engineering textbooks, which

explains that the calculation of a path loss can be done from a specified frequency linking two isotropic antennas or half-wave (λ/2) dipole. A bigger diameter antenna is more efficient with a greater gain than a narrower one as it receives more power from the moving radio signal. Nevertheless, multiple antennas may be grouped into the same area with shorter wavelengths. Other losses can occur in the event of reflection and diffraction, which is highly dependent on the material and its terrain. Even though the range of mm-Wave is reduced due to reflection and diffraction, they also facilitate non-line-of-sight interaction. And while low frequency signals can propagate through walls more efficiently, mm-Wave signals are almost impossible to propagate quite deep through most solid materials. Table 2.2 gives an insight on attenuation for different materials. Similarly, foliage losses for mm-Wave are significant and can impair propagation in some cases. mm-Wave transmissions can also experience substantial attenuations in the incidence of heavy rain. Raindrops can approximately be the same as radio wavelengths (millimeters) and as a result can cause scattering of the radio signal. However, as part of the design for MMB systems, a tool that would enable emergency communication across cellular bands when mm-Wave communication is disrupted due to heavy rain must be well thought out.

Table 2.2: Attenuation for different materials [55]

Material	**Thickness (cm)**	**Attenuation < 3 GHz [dB]**	**Attenuation 60 GHz [dB]**
Drywall	2.5	5.4	6
Office whiteboard	1.9	0.5	9.6
Clear glass	0.3/0.4	6.4	3.6
Mesh glass	0.3	7.7	10.2
Wood	0.7	5.4	-
Concrete	10	17.7	-

2.5 Hybrid Precoding

Hybrid precoding in mm-Wave MIMO systems is a recently emerged technique [14]-[18]. It is a mixture of both analog precoding and digital precoding. Essentially, for incoming data streams there is a precoding done at the baseband for the elimination of inter-symbol interference, the analog precoder then converts the digital data stream to the analog via a digital to analog converter. This precoder allows several changes between RF-controlled phase shifters and eventually enables the directional beam well into the medium to attain its optimum at the appropriate client position. Therefore, both the transmitter and the receiver use this coding mechanism. This approach, which has formerly been used exclusively for analog beamforming for a single-user will enable the system to send simultaneous data streams to various users. In essence, the hybrid precoder effectively allows sets of data to be transmitted to various users concurrently avoiding any possible interference.

In [13], a special case is presented by the optimal design, an instance, where RF chains are at least double the amount of streams of data. The main interference however that unravels this common situation is the fulfillment of unit modular limits of analog precoder. Orthogonal Matching Pursuit (OMP) is a commonly used hybrid precoding algorithms [11], that can help overpower this problem by confining analog precoding matrix columns as the subgroup of predetermined runner vectors. Although the design issue is considerably reduced, this additional constraint inevitably contributes to some loss of performance. In other terms, the generic hybrid precoding interface issue has still not been effectively resolved. Recently, more awareness has been concentrated on mainly limiting the computation complexity of OMP algorithm [19], [23], an example is, for every iteration the matrix inversion result is reused. However, the designing of

hybrid precoders codebook for narrowband and OFDM systems was presented in [24] and [25] respectively. Even though the design of the codebook was not quite complicated, and some performance losses were recorded, it remains unclear how much more performance gain can still be achieved.

2.6 Hybrid Precoding using Alternating Minimization Algorithms

AltMin is a super design approach that has been adopted to help break down the designing problem of a precoder into two larger problems, which is the analog and the digital precoder design. AltMin algorithm rotationally optimizes the analog precoder and the digital precoder. AltMin algorithm demonstrates that the analog precoder's unit modulus constraints define a Riemannian manifold. Therefore, the study also discusses AltMin algorithms focused on Manifold Optimizations (MO-AltMin). The algorithm would require no pre-established collection for analog precoders which by the way remains the earliest effort ever to decode the designing problems of hybrid precoding using the unit modulus constraint. Furthermore, by enforcing the digital precoding orthogonality properties, an algorithm called Phase Extraction based AltMin (PE-AltMin) can be discussed to function like a low complex match for the algorithm of the MO-AltMin, and this would in fact be more realistic to implement. Therefore, algorithms of MO-AltMin and PE-AltMin could commonly be used in OFDM-based and narrowband systems. Simulation results in Chapter 4, will reveal that a better solution can be resourcefully identified by MO-AltMin algorithm, meanwhile the existing OMP algorithm would be outmatched by a hands-on computational complexity of PE-AltMin algorithm.

Chapter 3

MILLIMETER-WAVE MIMO SYSTEMS AND PRECODING

In this chapter, four topics will be discussed. The first topic is the system model and problem formulation, under which system model, channel model and problem formulation will be conversed. The second topic will focus on manifold optimization-based hybrid precoding and under this topic, digital baseband precoders design is discussed, furthermore, analog RF precoders design via manifold optimization is also discussed, and lastly hybrid precoder design will also be discussed. The third topic will focus on low-complexity hybrid precoding, and under this topic, digital baseband precoder structure and hybrid precoder design will be discussed. And finally, the fourth topic will explore some critical areas under hybrid precoding in mm-Wave MIMO-OFDM systems.

3.1 System Model and Problem Formulation

In this section, firstly the system and channel models of the considered mm-Wave MIMO system will be discussed, and then formulation of problem for hybrid precoding will also be discussed.

3.1.1 System Model

As shown in Figure 1.3, considering a single-user mm-Wave MIMO system where N_s streams of data are transferred by N_t transmitting antennas and received by N_r receiving antennas. RF chain number is denoted as N_{RF}^{t} at the transmitter and N_{RF}^{r}, at

the receiver correspondingly, and is subjected to limitations $N_s \leq N_{\mathrm{RF}}^t \leq N_t$ and $N_s \leq N_{\mathrm{RF}}^r \leq N_r$.

The transmitted signal can be written as $\mathbf{x} = \mathbf{F}_{\mathrm{RF}}\mathbf{F}_{\mathrm{BB}}\mathbf{s}$, in which $\mathbf{s}$ represents $N_s \times 1$ symbols vectors such that $\mathrm{E}[\mathbf{s}\mathbf{s}^H] = \frac{1}{N_s}\mathbf{I}_{N_s}$. The hybrid precoder is made up of an $N_{\mathrm{RF}}^t \times N_s$ digital baseband precoder $\mathbf{F}_{\mathrm{BB}}$ and $N_t \times N_{\mathrm{RF}}^t$ of an analog RF precoders $\mathbf{F}_{\mathrm{RF}}$. The constraint in the transmit power can be given as $\|\mathbf{F}_{\mathrm{RF}}\mathbf{F}_{\mathrm{BB}}\|_{\mathrm{F}}^2 = N_s$. For clarity sake, we take into account a propagating channel for narrowband block-fading and the signal procured after homogenizing the process is specified as:

$$\mathbf{y} = \sqrt{\rho}\mathbf{W}_{\mathrm{BB}}^H\mathbf{W}_{\mathrm{RF}}^H\mathbf{H}\mathbf{F}_{\mathrm{RF}}\mathbf{F}_{\mathrm{BB}}\mathbf{s} + \mathbf{W}_{\mathrm{BB}}^H\mathbf{W}_{\mathrm{RF}}^H\mathbf{n}, \tag{3.1}$$

where ρ denote average power received, and $\mathbf{H}$ represents channel matrix, $\mathbf{W}_{\mathrm{BB}}$ is $N_{\mathrm{RF}}^r \times N_s$ digital baseband decoder, $\mathbf{W}_{\mathrm{RF}}$ is $N_r \times N_{\mathrm{RF}}^r$ of the receiver's analog RF decoder, and $\mathbf{n}$ represents noise vector of independent and identically distributed (i.i.d.) of the complex Gaussian distribution $CN(0, \sigma_{\mathrm{n}}^2)$ elements. Please note that N_{RF} is a sequence of electronic components and sub-units that include mixers, filters, amplifiers, attenuators and detectors. It allows passband communication signals to be processed at the baseband. In this study, it is believed that both the transmitters and the receivers are known to brilliant Channel State Information (CSI), and in reality, CSI could even be identified correctly but also effectively at the receiver's end by channel estimation [16] and with effective feedback techniques it can be further distributed at the transmission end [11], [28]. When the symbols that was transmitted obeys the normal distributions, spectral efficiency that are attainable may then be expressed as:

$$\mathrm{R} = \log\det\left(\mathbf{I}_{N_s} + \frac{\rho}{\sigma_{\mathrm{n}}^2 N_s}(\mathbf{W}_{\mathrm{RF}}\mathbf{W}_{\mathrm{BB}})^{+}\mathbf{H}\mathbf{F}_{\mathrm{RF}}\mathbf{F}_{\mathrm{BB}} \times \mathbf{F}_{\mathrm{BB}}^H\mathbf{F}_{\mathrm{RF}}^H\mathbf{H}^H(\mathbf{W}_{\mathrm{RF}}\mathbf{W}_{\mathrm{BB}})\right). \tag{3.2}$$

The analog precoding systems are used together with phase shifters that would only regulate the signal phases. Therefore, all unit modulus constraints should be met by non-zero $\mathbf{W}_{\mathrm{RF}}$ and $\mathbf{F}_{\mathrm{RF}}$, namely $\left|(\mathbf{W}_{\mathrm{RF}})_{i,j}\right| = \left|(\mathbf{F}_{\mathrm{RF}})_{i,j}\right| = 1$ for non-zero elements.

For the structure of Figure 1.3, each RF chain's output signal is transmitted over phase shifters to the entire antennas, and thus, for each RF chain, the structure has maximum beamforming gain with a regular combination of the antennas and RF chains, although, the complications of hardware implementation can be high.

3.1.2 Channel Model

mm-Wave propagation system, because of high free space losses, is clearly described as a model of cluster channel known as Saleh-Valenzuela [4]. This prototype shows the matrices of the mm-Wave channel as:

$$\mathbf{H} = \sqrt{\frac{N_t N_r}{\mathrm{N_{cl}} \mathrm{N_{ray}}}} \sum_{\mathrm{i}=1}^{\mathrm{N_{cl}}} \sum_{\mathrm{l}=1}^{\mathrm{N_{ray}}} \alpha_{\mathrm{il}} a_{\mathrm{r}} (\varphi_{\mathrm{il}}^{\mathrm{r}}, \theta_{\mathrm{il}}^{\mathrm{r}}) a_{\mathrm{t}} (\varphi_{\mathrm{il}}^{\mathrm{t}}, \theta_{\mathrm{il}}^{\mathrm{t}})^{H} \tag{3.3}$$

where within every cluster, the numbers of clusters and the number of rays symbolizes $\mathrm{N_{cl}}$ and $\mathrm{N_{ray}}$, and in the *i*th propagation cluster, the gain from the *l*th ray is denoted as α_{il}. This study assumes that α_{il} are random variables of i.i.d. that follows the complex Gaussian function $CN(0, \sigma_{\alpha,\mathrm{i}}^2)$ as well as $\sum_{\mathrm{i}=1}^{\mathrm{N_{cl}}} \sigma_{\alpha,\mathrm{i}}^2 = \hat{y}$, so that is in fact a normalizing factor that satisfies $\mathrm{E}\left[\|\mathbf{H}\|_F^2\right] = N_t N_r$. Furthermore, $a_{\mathrm{r}}(\varphi_{\mathrm{il}}^{\mathrm{r}}, \theta_{\mathrm{il}}^{\mathrm{r}})$ and $a_{\mathrm{t}}(\varphi_{\mathrm{il}}^{\mathrm{t}}, \theta_{\mathrm{il}}^{\mathrm{t}})$ indicate the received and transmitted array response vectors, where $\varphi_{\mathrm{il}}^{\mathrm{r}}(\varphi_{\mathrm{il}}^{\mathrm{t}})$ and $\theta_{\mathrm{il}}^{\mathrm{r}}(\theta_{\mathrm{il}}^{\mathrm{t}})$ represents azimuth and elevation Angles of Arrival (AoA) as well as Angles of Departure (AoD), respectively. In this study, the Uniform Square Planar Array (USPA) is considered with $\sqrt{\mathrm{N}} \times \sqrt{\mathrm{N}}$ elements of antenna where $N = N_t = N_r$. Hence, the vector of the array response matching the *l*th ray can be written in the *i*th cluster as:

$$a(\varphi_{il}\theta_{il}) = \frac{1}{\sqrt{N}} \exp\left\{ j \frac{2\pi}{\lambda} d(p \sin\varphi_{il} \sin\theta_{il} + q \cos\theta_{il}) \right\} \tag{3.4}$$

where λ denotes the signal wavelength and d signifies the antenna spacing, and 2D plane antenna indices can be expressed as $0 \leq p < \sqrt{\mathrm{N}}$ and $0 \leq q < \sqrt{\mathrm{N}}$. Although this channel model is used for simulations, but this precoding design approach applies to wide-ranging models.

3.1.3 Problem Formulation

In [11], it can be seen that precoding and decoding design may be divided across two distinct design problems: precoding problem and decoding problem. Both of them have almost the same carefully worked-out compositions apart from precoding that has supplementary power constraint. The precoder design in the rest of this study is therefore the main focus, and the algorithms are also applicable to the decoders. The homologous problem formulation is however specified accordingly via:

$$\begin{aligned} &\text{minimize } (\mathbf{F}_{\mathrm{RF}}, \mathbf{F}_{\mathrm{BB}}) \quad \left\|\mathbf{F}_{\mathrm{opt}} - \mathbf{F}_{\mathrm{RF}}\mathbf{F}_{\mathrm{BB}}\right\|_{\mathrm{F}} \\ &\text{subject to} \quad \begin{cases} \left|(\mathbf{F}_{\mathrm{RF}})_{ij}\right| = 1, \forall\, i, j, \\ \|\, \mathbf{F}_{\mathrm{RF}}\mathbf{F}_{\mathrm{BB}}\|_{\mathrm{F}}^{2} = N_s, \end{cases} \end{aligned} \tag{3.5}$$

in which $\mathbf{F}_{\mathrm{opt}}$ denotes the optimum fully digital precoder, whereas $\mathbf{F}_{\mathrm{RF}}$ and $\mathbf{F}_{\mathrm{BB}}$ are the analog and digital precoders to be optimized. Please note that, for point-to-point systems, SVD of a channel matrix determines $\mathbf{F}_{\mathrm{opt}}$. Furthermore, when the number of RF chains is equal to that of the antennas, it results in a high complex hardware and high power consumption for massive MIMO systems. Hence, the need for hybrid precoding emerges.

As seen in [11], curtailing the objective function in (3.5) contributes to spectral efficiency maximization. Furthermore, $\mathbf{F}_{\mathrm{opt}}$ matrix contains the first N_s columns of $\mathbf{V}$ and $\mathbf{U}$, that are in fact unitary matrix created out from SVD channel, such that, $\mathbf{H} = \mathbf{U}\boldsymbol{\Sigma}\mathbf{V}^{H}$.

In this study, problem (3.5) will be treated mainly as a problem of matrix factorization which involves two matrix parameters $\mathbf{F}_{\mathrm{RF}}$ and $\mathbf{F}_{\mathrm{BB}}$, using AltMin as key primary approach. Nonetheless, AltMin represents a commonly used and empirically efficient solution to the problems associated with the optimization of different subsets of variables. In various frameworks, which include matrices completions [29], phase recovery [30], image re-constructions [31], blind deconvolutions [32], factorization of non-negative matrix [33], AltMin approach was effectively applied. However, in the aforementioned variables $\mathbf{F}_{\mathrm{RF}}$ and $\mathbf{F}_{\mathrm{BB}}$, optimizing them jointly is extremely complex because of $\mathbf{F}_{\mathrm{RF}}$ element-wise unit modulus constraints. Thus, by decoupling them, alternating minimization comes off as an efficient way of achieving an efficient solution. Using the alternating minimization approach, $\mathbf{F}_{\mathrm{RF}}$ and $\mathbf{F}_{\mathrm{BB}}$ will be solved alternately while fixing the other, and this will essentially be the main idea throughout this study.

3.2 Hybrid Precoding focused on Manifold Optimization

In mm-Wave MIMO systems the structure in Figure 1.3 is constantly been used and this structure restricts any entry to become unit modulus in the analog precoding matrix, thereby rendering the precoder design problems unyielding by this element-wise restriction. In this study, an algorithm for AltMin grounded on the principles of manifold optimization will be explored explicitly in resolving (3.5), by showing that a Riemannian manifold can be described when there are limitations on the unit modulus.

Further so, authors in [13], as discussed by [34], showed that the Euclidean norm of (3.5) could be exactly zero given that $N_{\mathrm{RF}}^{t} \geq 2N_{s}$. This means that in this particular case the hybrid precoders are capable of performing in the capacity of the optimal

hybrid precoders as well as the fully digital precoder have been achieved by [13]. Consequently, this study will focused in the region where $N_s \leq N_{\mathrm{RF}}^t < 2N_s$.

3.2.1 Digital Baseband Precoder Design

Firstly, digital precoder $\mathbf{F}_{\mathrm{BB}}$ with a fixed analog precoder $\mathbf{F}_{\mathrm{RF}}$ has to be design. Therefore, problem (3.5) can be reiterated as:

$$\text{minimize } (\mathbf{F}_{\mathrm{BB}}) \left\|\mathbf{F}_{\mathrm{opt}} - \mathbf{F}_{\mathrm{RF}}\mathbf{F}_{\mathrm{BB}}\right\|_{\mathrm{F}}, \tag{3.6}$$

and the most common solution of the least squares is,

$$\mathbf{F}_{\mathrm{BB}} = \mathbf{F}_{\mathrm{RF}}^{+}\mathbf{F}_{\mathrm{opt}}. \tag{3.7}$$

Note that on the recipient side (3.7) has already given a widely-accepted ideal solution to the corresponding part of the design problem.

3.2.2 Analog RF Precoder Design via Manifold Optimization

$\mathbf{F}_{\mathrm{BB}}$ is fixed for the following interchanging phase, and search for an analog precoder to optimize the issue below:

$$\begin{aligned} &\text{minimize } (\mathbf{F}_{\mathrm{RF}}) \quad \left\|\mathbf{F}_{\mathrm{opt}} - \mathbf{F}_{\mathrm{RF}}\mathbf{F}_{\mathrm{BB}}\right\|_{\mathrm{F}}^2 \\ &\text{subject to} \qquad |(\mathbf{F}_{\mathrm{RF}})_{\mathrm{i,j}}| = 1, \forall\, \mathrm{i,j} \end{aligned} \tag{3.8}$$

The unit modulus constraints are the key stumbling block, that is, $|(\mathbf{F}_{\mathrm{RF}})_{\mathrm{i,j}}| = 1, \forall\, \mathrm{i,j}$, that are not essentially convex. There are no common methods in solving (3.8) in the best possible way, and that is perhaps the leading challenge of alternating minimization. An efficient algorithm focused on manifold optimization will be explored to find an almost optimal resolution to problem (3.8).

As seen in Figure 3.1, the Euclidean space is homeomorphic to each point in a manifold *M* [36]. On the point *x* of manifold *M*, the tangent space $\mathrm{T}_x M$ consist of tangent vector

ξ_x on the γ curls via x. In many real-life implementations, manifolds are categorized into different topological manifold called Riemannian manifold. An internal product that is well defined on the tangent space T_xM, regarded as the Riemannian metric, is equipped with Riemannian manifold. It allows measurements of angles and distances on manifolds to be taken. The calculus of a Riemannian manifold with Riemannian metric is therefore likely to be used. Furthermore, the gradients of cost functions can be defined with the help of rich geometry of Riemannian manifolds. Primarily, optimization over a Euclidean space with a smooth constraint is comparable locally to that of Riemannian manifold. Hence, Riemannian manifolds are used as a counterpart in the versed conjugate gradient algorithms of Euclidean spaces. Thus, as the section continues, this counterpart will be momentarily presented.

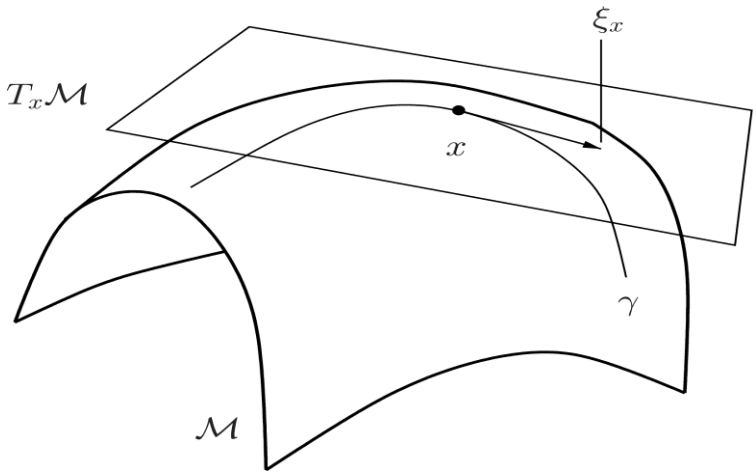

Figure 3.1: The tangent vector and space of a Riemannian manifold [35]

First the Euclidean metric and the complex plane C is provided as

$$\langle x_1, x_2 \rangle = \Re\{x_1^* x_2\}, \tag{3.9}$$

where C is equivalent to that of R^2 with the canonical internal product. Hence, the complex circle is represented as

$$\mathrm{M}_{cc} = \{x \in \mathrm{C} : x * x = 1\}. \quad (3.10)$$

The direction along which it can be traced is defined by tangent vectors given a number of points x over M_{cc} manifold. Therefore, the tangential area of the point $x \in \mathrm{M}_{cc}$ can be expressed in,

$$\mathrm{T_x M}_{cc} = \{z \in \mathrm{C} : \mathrm{z}^*\mathrm{x} + \mathrm{x}^*\mathrm{z} = 2\langle \mathrm{x}, \mathrm{z}\rangle = 0\}. \quad (3.11)$$

Bear in mind that a vector $\mathbf{x} = \mathrm{vec}(\mathbf{F}_{\mathrm{RF}})$ generates a manifold of complex circle $\mathrm{M}_{\mathrm{cc}}^{\mathrm{m}} = \{x \in \mathrm{C}^{\mathrm{m}} : |\mathrm{x}_1| = |\mathrm{x}_2| = \cdots = |\mathrm{x}_{\mathrm{m}}| = 1\}$, where $m = N_{\mathrm{t}}N_{\mathrm{RF}}^{t}$. Hence, the optimizing problems exploration area (3.8) is over the product of a complex level of m circles, that remains a C^{m} sub-manifold from Riemannian and the product geometry. Therefore, at a known point, the tangential space $x \in \mathrm{M}_{\mathrm{cc}}^{\mathrm{m}}$ may be described in the following:

$$\mathrm{T_x M}_{\mathrm{cc}} = \{z \in \mathrm{C}^{\mathrm{m}} : \Re\{z \circ x^*\} = 0_m\}. \quad (3.12)$$

The negative Riemannian gradients, identical to Euclidean space, are connected to one of all tangent vectors, which reflects that path of the ultimate decline in function. Therefore, as a Riemannian sub Manifold of C^{m} is a complex circle M_{cc} manifold, the gradient of Riemannian of x was the tangent vector grad $f(x)$ generated from the orthogonality projections by Euclidean gradient $\nabla f(x)$ along a tangential area $\mathrm{T_x M}_{\mathrm{cc}}^{\mathrm{m}}$ [35]:

$$\begin{aligned} \mathrm{grad}\, f(x) &= \mathrm{Proj}_x \nabla f(x) \\ &= \nabla f(x) - \Re\{\nabla \mathrm{f(x)} \circ x^*\} \circ x. \end{aligned} \quad (3.13)$$

For which, the cost functions from the gradients of Euclidean in (3.8) can be expressed as:

$$\nabla f(x) = -2(\mathbf{F}_{\mathrm{BB}}^{*} \otimes \mathbf{I}_{N_t})\left[\mathrm{vec}\left(\mathbf{F}_{\mathrm{opt}}\right) - (\mathbf{F}_{\mathrm{BB}}^{\mathrm{T}} \otimes \mathbf{I}_{N_t})\mathbf{x}\right]. \quad (3.14)$$

Please note, details on the use of certain techniques for complex-valued matrix derivatives for resolving Euclidean gradient is available in [38].

Another important element of manifold optimization is retraction. It draws a vector to the manifold itself from the tangent space and can also determine the targeted point along the manifold when moving on a tangent vector. However, the tangent vector retraction $\boldsymbol{\alpha}\mathbf{d}$ at point $x \in \mathrm{M}_{\mathrm{cc}}^{\mathrm{m}}$ could be defined as:

$$\mathrm{Retr}_{\mathbf{x}} : \mathrm{T}_{\mathrm{x}}\mathrm{M}_{\mathrm{cc}}^{\mathrm{m}} \rightarrow \mathrm{M}_{\mathrm{cc}}^{\mathrm{m}}:$$

$$\boldsymbol{\alpha}\mathbf{d} \rightarrow \mathrm{Retr}_{\mathbf{x}}(\boldsymbol{\alpha}\mathbf{d}) = \mathrm{vec}\left[\frac{(\mathbf{x} + \boldsymbol{\alpha}\mathbf{d})_i}{|(\mathbf{x} + \boldsymbol{\alpha}\mathbf{d})_i|}\right]. \quad (3.15)$$

Provided with Riemannian gradient, tangent space, and retractions of a complex circle $\mathrm{M}_{\mathrm{cc}}^{\mathrm{m}}$ manifolds, a conjugate gradient method based on the line exploration [39], which in Euclidean space is a standard algorithm that could be better developed for the designing of analog precoding as seen in the first process below.

Algorithm 1: Manifold Optimization for Analog Precoding using Conjugate Gradient Algorithm

Input: $\mathbf{F}_{\mathrm{BB}}$, $\mathbf{F}_{\mathrm{opt}}$, $\mathbf{x}_0 \in \mathrm{M}_{\mathrm{cc}}^{\mathrm{m}}$

1. $\mathbf{d_0}$ = -grad $f(\mathbf{x}_0)$ also $k = 0$
2. **Repeats**
3. Select a line search based Armijo backtracking with step size α_k;
4. Look for the next point $\mathbf{x}_{k+1}$by making use of retraction in (3.15): $\mathbf{x}_{k+1}$ = $\mathrm{Retr}_{\mathbf{x}_k}(\alpha_k \mathbf{d}_k)$;

5. Determine Riemannian gradient $\mathbf{g}_{k+1}$ = grad $f(\mathbf{x}_{k+1})$ according to (3.13) and (3.14);
6. Calculating vector transport $\mathbf{g}_k^+$ and $\mathbf{d}_k^+$ of gradient $\mathbf{g}_k$ and direction of conjugate $\mathbf{d}_k$ from $\mathbf{x}_k$ to $\mathbf{x}_{k+1}$;
7. Select parameter for Polak-Ribiere β_{k+1};
8. Determine direction of conjugate $\mathbf{d}_{k+1} = -\mathbf{g}_{k+1} + \beta_{k+1}\mathbf{d}_k^+$;
9. Then $k \leftarrow k + 1$
10. **Until** the stop criterion is triggered

Algorithm 1 makes use of the most well-known line search based Armijo backtracking step and parameters of Polak-Ribiere to ensure that the objective function in each iteration is not increasing. Please note that the stopping criterion is the iteration number exceeding a specified value α or the relative difference between two consecutive iterations becoming smaller than a specified value δ. For example, good performance can be achieved when we set $\delta = 10^{-5}$ according to the observation in simulations of Chapter 4. Furthermore, steps 7 and 8 encompass the set-ups in different various tangent spaces of two separate vectors $T_{x_k}\mathrm{M}_{\mathrm{cc}}^{\mathrm{m}}$ and $T_{x_{k+1}}\mathrm{M}_{\mathrm{cc}}^{\mathrm{m}}$, and cannot be joint directly, transport is then implemented and is simply mapped by two tangential vectors in separate tangential space. The transport from $\mathbf{x}_k$ to $\mathbf{x}_{k+1}$ of a tangent vector $\mathbf{d}$ can be stated as:

$$\mathrm{Trans}\,\mathrm{p}_{\mathbf{x}_k \to \mathbf{x}_{k+1}} : T_{x_k}\mathrm{M}_{\mathrm{cc}}^{\mathrm{m}} \to T_{x_{k+1}}\mathrm{M}_{\mathrm{cc}}^{\mathrm{m}} : \mathbf{d} \to \mathbf{d} - \Re\{\mathbf{d} \circ \mathbf{x}_{k+1}^*\} \circ \mathbf{x}_{k+1}, \quad (3.16)$$

which can be achieved in step 6. Algorithm 1 is certain to come together at a critical point, in which the gradients of the objective functions are zero [35].

3.2.3 Hybrid Precoding Design

In MO-AltMin algorithm the design of hybrid precoder through alternating minimization is described by problem-solving of (3.6) and (3.8) iteratively. To balance the power constraint in (3.5), $\mathbf{F}_{\mathrm{BB}}$ is normalized by a factor of $\frac{\sqrt{N_s}}{\|\mathbf{F}_{\mathrm{RF}}\mathbf{F}_{\mathrm{BB}}\|_{\mathrm{F}}}$ in step 7. The next proposition will help to illustrate the effect of normalization.

Algorithm 2: Algorithm of MO-AltMin for Hybrid Precoder Design using Manifold Optimization

Input: $\mathbf{F}_{\mathrm{opt}}$

1. Construct $\mathbf{F}_{\mathrm{RF}}^{(0)}$ with unusual stages and make *k = 0*;
2. **Repeats**
3. Select $\mathbf{F}_{\mathrm{RF}}^{(k)}$, and $\mathbf{F}_{\mathrm{BB}}^{(k)} = \mathbf{F}_{\mathrm{RF}}^{(k)+}\mathbf{F}_{\mathrm{opt}}$;
4. $\mathbf{F}_{\mathrm{RF}}^{(k+1)}$ by making use of Algorithm 1 when $\mathbf{F}_{\mathrm{BB}}^{(k)}$ is selected;
5. Then $k \leftarrow k$ +1;
6. **Until** the stop condition is triggered
7. At transmitting end, normalize $\hat{\mathbf{F}}_{\mathrm{BB}} = \frac{\sqrt{N_s}}{\|\mathbf{F}_{\mathrm{RF}}\mathbf{F}_{\mathrm{BB}}\|_{\mathrm{F}}}\mathbf{F}_{\mathrm{BB}}$ for the digital precoder.

Proposition 1: If the distance of Euclidean preceding normalization stays as $\left\|\mathbf{F}_{\mathrm{opt}} - \mathbf{F}_{\mathrm{RF}}\mathbf{F}_{\mathrm{BB}}\right\|_{\mathrm{F}} \leq \delta$, then after normalization, we have $\left\|\mathbf{F}_{\mathrm{opt}} - \mathbf{F}_{\mathrm{RF}}\hat{\mathbf{F}}_{\mathrm{BB}}\right\|_{\mathrm{F}} \leq 2\delta$

Proof: Defining normalization factor $\frac{\sqrt{N_s}}{\|\mathbf{F}_{\mathrm{RF}}\mathbf{F}_{\mathrm{BB}}\|_{\mathrm{F}}} = \frac{1}{\lambda}$ and thus $\|\mathbf{F}_{\mathrm{RF}}\mathbf{F}_{\mathrm{BB}}\|_{\mathrm{F}} = \lambda\left\|\mathbf{F}_{\mathrm{opt}}\right\|_{\mathrm{F}}$.

By inequality of the norm,

$$\left\|\mathbf{F}_{\mathrm{opt}} - \mathbf{F}_{\mathrm{RF}}\mathbf{F}_{\mathrm{BB}}\right\|_{\mathrm{F}} \geq \left|\left\|\mathbf{F}_{\mathrm{opt}}\right\|_{\mathrm{F}} - \|\mathbf{F}_{\mathrm{RF}}\mathbf{F}_{\mathrm{BB}}\|_{\mathrm{F}}\right| = |1-\lambda|\left\|\mathbf{F}_{\mathrm{opt}}\right\|_{\mathrm{F}}, \quad (3.17)$$

and it is equal to $\left\|\mathbf{F}_{\text{opt}}\right\|_{\text{F}} \leq \frac{1}{|\lambda-1|}\delta$.

When $\lambda \neq 1$, it specifies that $\left\|\mathbf{F}_{\text{opt}} - \mathbf{F}_{\text{RF}}\mathbf{F}_{\text{BB}}\right\|_{\text{F}} \neq 0$,

$$\left\|\mathbf{F}_{\text{opt}} - \mathbf{F}_{\text{RF}}\hat{\mathbf{F}}_{\text{BB}}\right\|_{\text{F}}$$

$$= \left\|\mathbf{F}_{\text{opt}} - \mathbf{F}_{\text{RF}}\mathbf{F}_{\text{BB}} + \left(1 - \frac{1}{\lambda}\right)\mathbf{F}_{\text{RF}}\mathbf{F}_{\text{BB}}\right\|_{\text{F}} \leq \left\|\mathbf{F}_{\text{opt}} - \mathbf{F}_{\text{RF}}\mathbf{F}_{\text{BB}}\right\|_{\text{F}} + \left|1 - \frac{1}{\lambda}\right| \left\|\mathbf{F}_{\text{RF}}\mathbf{F}_{\text{BB}}\right\|_{\text{F}}$$

$$\leq \delta + |\lambda - 1|\left\|\mathbf{F}_{\text{opt}}\right\|_{\text{F}} \leq \delta + \frac{|\lambda-1|}{|\lambda-1|}\,\delta = 2\delta \tag{3.18}$$

If the distance of Euclidean between the hybrid precoders and the optimal digital precoder can be reduced enough to overcome the power constraint in (3.5), a small distance between the normalization step and optimal digital precoder can come to reality. Thus, each iteration will by no means increase it, if in problem (3.5) the objective function could be reduced in stages 3 and 4. Moreover, the objective function stays positive. Those two characteristics will combine to ensure a viable solution for MO-AltMin algorithm. However, for over-all non-convex issues, the optimality of AltMin algorithms remains an open problem [40]. Although, the complexity of the MO-AltMin algorithm is relatively high, therefore, in each iteration, the update of the analog precoder implicates a line search using Algorithm 1, thus, the fixed loop in MO-AltMin algorithm will cause the whole solving process to decelerate. In addition, end results of Kronecker products in (3.14) will be two matrices of dimension $N_t N_{\text{RF}}^t$ $\times$ $N_s N_t$, both of which will scale with the size of the antenna and later result in a computational complexity of MO-AltMin algorithm that grows rapidly. While highly complex, it is observed that under unit modulus constraints the hybrid precoder design problem in (3.5) can be directly solved by the manifold optimization based MO-AltMin algorithm and with this, it improves the spectral efficiency when compared with other current algorithms. Consequently, algorithm of MO-AltMin could be

offered as a benchmark as far as improving spectral efficiency is concern. Low-complexity algorithm however will be explored in the coming section.

3.3 Low-Complexity Hybrid Precoding

Even though MO-AltMin algorithm is capable of handling the limitations of unit modulus, owing to the vast nature of an antenna array, the quantity of such constraints may be considerably high. The high computational complexity will therefore stop its hands-on application. However, as a result of applying the orthogonal properties of the digital precoders, in this section, a low complexity design is discussed for the analog precoders determined by the limitations on the unit modulus. The analog precoder platforms can be obtained through corresponding precoder platforms that are defined by digital precoders and unregulated optimal precoders. This is as a result of the orthogonality properties of the digital precoders. Although there will be more performance losses in comparison to the algorithm of MO-AltMin, the results of the simulation, however, would show its gains in terms of performance over the already standing algorithm.

3.3.1 Structure of Digital Base-band Precoders

In order to mitigate interferences between multiplexed sources, the columns in $\mathbf{F}_{\mathrm{opt}}$ optimal precoding matrix must be equally orthogonal. Consequently, a comparable limitation is established where columns of the matrix of the digital precoding have to be orthogonally exclusive to each other as

$$\mathbf{F}_{\mathrm{BB}}^{H}\mathbf{F}_{\mathrm{BB}} = \alpha\mathbf{F}_{\mathrm{DD}}^{H}\alpha\mathbf{F}_{\mathrm{DD}} = \alpha^{2}\mathbf{I}_{N_s}, \tag{3.19}$$

where $\mathbf{F}_{\mathrm{DD}}$ has the same dimension as $\mathbf{F}_{\mathrm{BB}}$ and it is also a unitary matrix. Though there is no clear result on how digital precoder is structured in hybrid precoding, it is just normal and interesting to study the design of the hybrid precoder under a digital

orthogonal constraint. Moreover, such orthogonal constraint provides $\mathbf{F}_{\mathrm{RF}}$ analog precoder's capacity for removing $\mathbf{F}_{\mathrm{BB}}$ product shape that will greatly facilitates the design of the analog precoder.

3.3.2 Hybrid Precoder Design

By substituting $\mathbf{F}_{\mathrm{BB}}$ for $\alpha\mathbf{F}_{\mathrm{DD}}$, additional modification can be done on the objective function in (3.5) as:

$$\begin{aligned}\left\|\mathbf{F}_{\mathrm{opt}}-\mathbf{F}_{\mathrm{RF}}\mathbf{F}_{\mathrm{BB}}\right\|_{\mathrm{F}}^{2} &= \mathrm{Tr}\left(\mathbf{F}_{\mathrm{opt}}^{H}\mathbf{F}_{\mathrm{opt}}\right)-\mathrm{Tr}\left(\mathbf{F}_{\mathrm{opt}}^{H}\mathbf{F}_{\mathrm{RF}}\mathbf{F}_{\mathrm{BB}}\right)-\mathrm{Tr}\left(\mathbf{F}_{\mathrm{BB}}^{H}\mathbf{F}_{\mathrm{RF}}^{H}\mathbf{F}_{\mathrm{opt}}\right)\\ &\quad+\mathrm{Tr}\left(\mathbf{F}_{\mathrm{BB}}^{H}\mathbf{F}_{\mathrm{RF}}^{H}\mathbf{F}_{\mathrm{RF}}\mathbf{F}_{\mathrm{BB}}\right)\\ &= \left\|\mathbf{F}_{\mathrm{opt}}\right\|_{\mathrm{F}}^{2}-2\alpha\Re\mathrm{Tr}\left(\mathbf{F}_{\mathrm{DD}}\mathbf{F}_{\mathrm{opt}}^{H}\mathbf{F}_{\mathrm{RF}}\right)+\alpha^{2}\|\mathbf{F}_{\mathrm{RF}}\mathbf{F}_{\mathrm{DD}}\|_{\mathrm{F}}^{2}. \qquad (3.20)\end{aligned}$$

Evidently, once $\alpha=\frac{\Re\mathrm{Tr}\left(\mathbf{F}_{\mathrm{DD}}\mathbf{F}_{\mathrm{opt}}^{H}\mathbf{F}_{\mathrm{RF}}\right)}{\|\mathbf{F}_{\mathrm{RF}}\mathbf{F}_{\mathrm{DD}}\|_{\mathrm{F}}^{2}}$, the objective function $\left\|\mathbf{F}_{\mathrm{opt}}-\mathbf{F}_{\mathrm{RF}}\mathbf{F}_{\mathrm{BB}}\right\|_{\mathrm{F}}^{2}$ in (3.20) will have the least value, specified as $\left\|\mathbf{F}_{\mathrm{opt}}\right\|_{\mathrm{F}}^{2}-\frac{\left\{\Re\mathrm{Tr}\left(\mathbf{F}_{\mathrm{DD}}\mathbf{F}_{\mathrm{opt}}^{H}\mathbf{F}_{\mathrm{RF}}\right)\right\}^{2}}{\|\mathbf{F}_{\mathrm{RF}}\mathbf{F}_{\mathrm{DD}}\|_{\mathrm{F}}^{2}}$. Please note the square of Frobenius norm (also known as Euclidean norm) $\|\mathbf{F}_{\mathrm{RF}}\mathbf{F}_{\mathrm{DD}}\|_{\mathrm{F}}^{2}$ has the following upper bound:

$$\begin{aligned}\|\mathbf{F}_{\mathrm{RF}}\mathbf{F}_{\mathrm{DD}}\|_{\mathrm{F}}^{2} &= \mathrm{Tr}\left(\mathbf{F}_{\mathrm{DD}}^{H}\mathbf{F}_{\mathrm{RF}}^{H}\mathbf{F}_{\mathrm{RF}}\mathbf{F}_{\mathrm{DD}}\right)\\ &= \mathrm{Tr}\left\{\begin{pmatrix}\mathbf{I}_{N_s} & \\ & 0\end{pmatrix}\mathbf{K}^{H}\mathbf{F}_{\mathrm{RF}}^{H}\mathbf{F}_{\mathrm{RF}}\mathbf{K}\right\}\leq\mathrm{Tr}\{\mathbf{K}^{H}\mathbf{F}_{\mathrm{RF}}^{H}\mathbf{F}_{\mathrm{RF}}\mathbf{K}\}\\ &= \|\mathbf{F}_{\mathrm{RF}}\|_{\mathrm{F}}^{2} \qquad (3.21)\end{aligned}$$

where $\mathbf{F}_{\mathrm{DD}}^{H}\mathbf{F}_{\mathrm{DD}}=\mathbf{K}^{H}\begin{pmatrix}\mathbf{I}_{N_s} & \\ & 0\end{pmatrix}.\mathbf{K}$ will be SVD of $\mathbf{F}_{\mathrm{DD}}^{H}\mathbf{F}_{\mathrm{DD}}$ and the equality is maintained if and only if $N_{\mathrm{RF}}^{t}=N_s$ such that $\mathbf{F}_{\mathrm{DD}}$ is a square matrix. Therefore, in (3.5) the objective functions is upper bounded over $\left\|\mathbf{F}_{\mathrm{opt}}\right\|_{\mathrm{F}}^{2}-\frac{\left\{\Re\mathrm{Tr}\left(\mathbf{F}_{\mathrm{DD}}\mathbf{F}_{\mathrm{opt}}^{H}\mathbf{F}_{\mathrm{RF}}\right)\right\}^{2}}{\|\mathbf{F}_{\mathrm{RF}}\|_{\mathrm{F}}^{2}}$. To make

$\mathbf{F}_{\mathrm{RF}}$ eliminate its product form with $\mathbf{F}_{\mathrm{BB}}$ the constant term $\left(\frac{1}{2\|\mathbf{F}_{\mathrm{RF}}\|_{\mathrm{F}}^{2}}-1\right)\|\mathbf{F}_{\mathrm{opt}}\|_{\mathrm{F}}^{2}+\frac{1}{2}$ is added to the bound and then multiply it by $2\|\mathbf{F}_{\mathrm{RF}}\|_{\mathrm{F}}^{2}$. Then,

$$\begin{aligned}&\|\mathbf{F}_{\mathrm{opt}}\|_{\mathrm{F}}^{2}-2\Re\mathrm{Tr}\left(\mathbf{F}_{\mathrm{DD}}\mathbf{F}_{\mathrm{opt}}^{H}\mathbf{F}_{\mathrm{RF}}\right)+\|\mathbf{F}_{\mathrm{RF}}\|_{\mathrm{F}}^{2}\\&=\mathrm{Tr}(\mathbf{F}_{\mathrm{RF}}^{H}\mathbf{F}_{\mathrm{RF}})-2\Re\mathrm{Tr}\left(\mathbf{F}_{\mathrm{DD}}\mathbf{F}_{\mathrm{opt}}^{H}\mathbf{F}_{\mathrm{RF}}\right)+\mathrm{Tr}(\mathbf{F}_{\mathrm{DD}}\mathbf{F}_{\mathrm{opt}}^{H}\mathbf{F}_{\mathrm{opt}}\mathbf{F}_{\mathrm{DD}}^{H})\\&=\|\mathbf{F}_{\mathrm{opt}}\mathbf{F}_{\mathrm{DD}}^{H}-\mathbf{F}_{\mathrm{RF}}\|_{\mathrm{F}}^{2}.\end{aligned}\tag{3.22}$$

High complexity will still be an issue for optimizing the objective function in (3.20) directly, thus, in (3.22), rather than the upper bound adopting the original one, it adopts the objective function. Furthermore, by normalization, after hybrid precoders are updated the limitations on the transmitting power can be satisfied just like in MO-AltMin algorithm and Proposition 1, thus momentarily, the power constraint is removed. Hence, by embracing (3.22) to be an objective function, designing problem of the hybrid precoder can be stated as:

$$\begin{aligned}&\text{minimize } (\mathbf{F}_{\mathrm{RF}}\mathbf{F}_{\mathrm{DD}})\ \ \|\mathbf{F}_{\mathrm{opt}}\mathbf{F}_{\mathrm{DD}}^{H}-\mathbf{F}_{\mathrm{RF}}\|_{\mathrm{F}}^{2}\\&\text{subject to}\quad\begin{cases}\left|(\mathbf{F}_{\mathrm{RF}})_{ij}\right|=1,\forall\, i,j,\\\|\,\mathbf{F}_{\mathrm{DD}}^{H}\mathbf{F}_{\mathrm{DD}}\|_{\mathrm{F}}^{2}=\mathbf{I}_{N_s},\end{cases}\end{aligned}\tag{3.23}$$

The problem formulated in (3.23) indicates that we just have to find a unitary $\mathbf{F}_{\mathrm{DD}}$ precoding matrix, and that the orthogonal columns are then able to achieve an equivalent $\mathbf{F}_{\mathrm{BB}}$ precoding matrix. When alternating minimization is applied, the objective function in (3.23) considerably simplifies the design of the analog precoders. More importantly as $\mathbf{F}_{\mathrm{RF}}$ matrix eliminates the product form with $\mathbf{F}_{\mathrm{BB}}$, then a solution in closed form is established.

$$\arg(\mathbf{F}_{\mathrm{RF}})=\arg\left(\mathbf{F}_{\mathrm{opt}}\mathbf{F}_{\mathrm{DD}}^{H}\right),\tag{3.24}$$

for which, arg($\mathbf{F}_{\mathrm{RF}}$) creates matrices that is made up of phases of $\mathbf{F}_{\mathrm{RF}}$ entries. Hence, it demonstrates how $\mathbf{F}_{\mathrm{RF}}$ parts can be hauled out from the corresponding precoder parts $\mathbf{F}_{\mathrm{opt}}\mathbf{F}_{\mathrm{DD}}^{H}$. Similarly, solutions in closed form could be $\mathbf{F}_{\mathrm{opt}}\mathbf{F}_{\mathrm{DD}}^{H}$ of Euclidean projection on the analog precoder of the viable $\mathbf{F}_{\mathrm{RF}}$set.

In attempting to resolve $\mathbf{F}_{\mathrm{RF}}$ digital precoder, the following issue is optimized

$$\begin{aligned} &\text{minimize } (\mathbf{F}_{\mathrm{DD}}) \quad \left\|\mathbf{F}_{\mathrm{opt}}\mathbf{F}_{\mathrm{DD}}^{H} - \mathbf{F}_{\mathrm{RF}}\right\|_{\mathrm{F}}^{2} \\ &\text{subject to} \qquad \mathbf{F}_{\mathrm{DD}}^{H}\mathbf{F}_{DD} = \mathbf{I}_{N_s}. \end{aligned} \tag{3.25}$$

As the problem (3.25) has only one $\mathbf{F}_{\mathrm{DD}}$ optimization variable, this corresponds to

$$\begin{aligned} &\text{maximize } (\mathbf{F}_{\mathrm{DD}}) \quad \Re\mathrm{Tr}\left(\mathbf{F}_{\mathrm{DD}}\mathbf{F}_{\mathrm{opt}}^{H}\mathbf{F}_{\mathrm{RF}}\right) \\ &\text{subject to} \qquad \mathbf{F}_{\mathrm{DD}}^{H}\mathbf{F}_{\mathrm{DD}} = \mathbf{I}_{N_s}. \end{aligned} \tag{3.26}$$

In line with the dual norm interpretation,

$$\begin{aligned} \Re\mathrm{Tr}\left(\mathbf{F}_{\mathrm{DD}}\mathbf{F}_{\mathrm{opt}}^{H}\mathbf{F}_{\mathrm{RF}}\right) &\leq \left|\mathrm{Tr}\left(\mathbf{F}_{\mathrm{DD}}\mathbf{F}_{\mathrm{opt}}^{H}\mathbf{F}_{\mathrm{RF}}\right)\right| \leq^{(a)} \|\mathbf{F}_{\mathrm{DD}}^{H}\|_{\infty} \cdot \left\|\mathbf{F}_{\mathrm{opt}}^{H}\mathbf{F}_{\mathrm{RF}}\right\|_{1} \\ &= \left\|\mathbf{F}_{\mathrm{opt}}^{H}\mathbf{F}_{\mathrm{RF}}\right\|_{1} = \sum_{i=1}^{N_s}\sigma_i. \end{aligned} \tag{3.27}$$

Thus (a) corresponds to the inequality of Hölder, $\|\cdot\|_1$ stands for one and norms of infinite Schatten is represented as $\|\cdot\|_\infty$. The establishment of equality can only be possible when

$$\mathbf{F}_{\mathrm{DD}} = \mathbf{V}_1\mathbf{U}^{H} \tag{3.28}$$

where $\mathbf{F}_{\mathrm{opt}}^{H}\mathbf{F}_{\mathrm{RF}} = \mathbf{U}\sum\mathbf{V}^{H} = \mathbf{U}\mathbf{S}\mathbf{V}_1^{H} = \mathrm{SVD}$, $\mathbf{S}$ stands for diagonal matrix and its elements represents the opening N_s nonzero singular values $\sigma_1,\ldots,\sigma_{N_s}$.

Algorithm 3: Algorithm for PE-AltMin acting as low-complexity algorithm

Inputs: $\mathbf{F}_{\mathrm{opt}}$

1. Construct $\mathbf{F}_{\mathrm{RF}}^{(0)}$ with unusual phases and make $k = 0$;
2. **Repeats**
3. Select $\mathbf{F}_{\mathrm{RF}}^{(\mathrm{k})}$, determine SVD: $\mathbf{F}_{\mathrm{opt}}^{H}\mathbf{F}_{\mathrm{RF}}^{(\mathrm{k})} = \mathbf{U}^{(\mathrm{k})}\mathbf{S}^{(\mathrm{k})}\mathbf{V}_{1}^{(\mathrm{k})^{\mathrm{H}}}$;
4. $\mathbf{F}_{\mathrm{DD}}^{(\mathrm{k})} = \mathbf{V}_{1}^{(\mathrm{k})}\mathbf{U}^{(\mathrm{k})^{\mathrm{H}}}$;
5. Select $\mathbf{F}_{\mathrm{DD}}^{(\mathrm{k})}$ and $\arg\left\{\mathbf{F}_{\mathrm{RF}}^{(\mathrm{k}+1)}\right\} = \arg\left(\mathbf{F}_{\mathrm{opt}}\mathbf{F}_{\mathrm{DD}}^{(\mathrm{k})^{\mathrm{H}}}\right)$;
6. Then $k \leftarrow k + 1$;
7. **Until** the stop condition is triggered
8. At transmitting end, normalize $\hat{\mathbf{F}}_{BB} = \frac{\sqrt{N_S}}{\|\mathbf{F}_{\mathrm{RF}}\mathbf{F}_{\mathrm{DD}}\|_{\mathrm{F}}}\mathbf{F}_{\mathrm{DD}}$ for the digital precoder

Thus, on the basis of the two solutions in closed form to both digital precoder as well as analog precoder, PE-AltMin algorithm is brought to light. The algorithm of PE-AltMin however has numerous concerns that need some more observations.

1) **Complexity**: The guidelines of upgrading digitized precoders are governed by means of a solution in closed form in either algorithm of PE-AltMin or that of MO-AltMin, thus making both algorithms have related complexity in terms of digital functionality. Also, the dimension of the digital precoder in a hybrid precoding system is far below that of the analog precoder, and this makes the analog part to lead the algorithms complexity.

   In every MO-AltMin algorithm iteration, every iteration carried out on analog precoder may be upgraded by continuously searching the complex circle manifold in order to obtain the optimal locality without any gradient of its cost

functions. In addition, the computing of large size $N_t N_{\mathrm{RF}}^t \times N_s N_t$ dimensional matrices is entangled within the techniques of the gradient descent because Kronecker products is used. Furthermore, the iterative procedure of the conjugated form of the gradient descent is fixed within every iteration of alternating minimization and this fixed structure of iteration reduces considerably the computational effectiveness of MO-AltMin. Conversely, the phase extracting process of the matrix $\mathbf{F}_{\mathrm{opt}}\mathbf{F}_{\mathrm{DD}}^H$ can cause modification on the analog precoder at each PE-AltMin algorithm iteration, with a dimension of $N_t \times N_{\mathrm{RF}}^t$. It may also be said that PE-AltMin algorithm is significantly less complex, as shown numerically from simulation results, with respect to MO-AltMin algorithm.

2) **Approximation Accuracy:** In (3.23), effort was made not to explicitly reduce the original objective function, but to decrease the upper bound as specified by (3.21). The importance of a strategy like the aforementioned one therefore relies on the compactness of the upper limit such that $N_s \leq N_{\mathrm{RF}}^t < 2N_s$. With respects to (3.21), we can quantify the gap between $\|\mathbf{F}_{\mathrm{RF}}\mathbf{F}_{\mathrm{DD}}\|_{\mathrm{F}}^2$ and $\|\mathbf{F}_{\mathrm{RF}}\|_{\mathrm{F}}^2$ as $\|\mathbf{F}_{\mathrm{RF}}\mathbf{K}_1\|_{\mathrm{F}}^2$, for which $\mathbf{K}_1$ is composed of the rightmost $N_{\mathrm{RF}}^t - N_s$ $\mathbf{K}$ column. Observe that, while $N_{\mathrm{RF}}^t = N_s$, the upper bound becomes compact, such that, in (3.21) equality holds. Moreover, when N_{RF}^t is increased from N_s to $2N_s - 1$, the gap $\|\mathbf{F}_{\mathrm{RF}}\mathbf{K}_1\|_{\mathrm{F}}^2$ becomes greater with an increasing N_{RF}^t, which leads to performance losses. In the simulation results, the consequence of using top limits as benchmarks can be seen.

3) **Calculation of α:** Although α-value may be determined to create an equivalent $\mathbf{F}_{\mathrm{BB}}$ matrix for every $\mathbf{F}_{\mathrm{DD}}$ as previously stated, the calculation of α in PE-AltMin algorithm is not necessary because of the following. On the

transmitting side, if, at the last step of the algorithm of PE-AltMin, $\mathbf{F}_{BB} = \alpha\mathbf{F}_{DD}$ is calculated, the digital precoder has indeed been promptly normalised. Therefore, the entire process is equitable to normalizing $\mathbf{F}_{DD}$ instantly to meet the energy restriction, in the absence of knowing what α is. From the receiving side, it is observed that the spectral efficiency would not be impacted when $\mathbf{W}_{BB}$ multiplies α, the constant factor in (3.2), since the decoder $\mathbf{W}_{BB}$ affects both the noise and the received signal, hence, with the constant factor α, Signal-to-Noise Ratio (SNR) will remain the same. Note that, escaping α calculation will help further to alleviate the difficulty of the algorithm of PE-AltMin.

3.4 Hybrid Precoding for mm-Wave MIMO-OFDM System

Hybrid precoding for narrowband mm-Wave system was discussed in previous sections. However, the huge accessible bandwidth is a key distinctive feature of mm-Wave technologies and as such, while utilizing multi-carrier strategies including OFDM to prevent multi-path fading, the hybrid precoders layout must also be discussed. This section shows how algorithms of AltMin could be incorporated into MIMO-OFDM mm-Wave models.

The digital precoding of every single sub-carrier is carried out in the frequency domain in typical MIMO-OFDM schemes with a carrier frequency of sub 6 GHz and could be utilized in a MIMO-OFDM mm-Wave model. More so, the Inverse Fast Fourier Transform (IFFT) is trailing digital precoding, which brings together signals from the entire sub-carriers. The outcome of a post-IFFT procedure is, therefore, analog precoding, so the entire sub-carriers signals in mm-Wave MIMO-OFDM systems shares just one mutual analog precoder [20]. Subject to this limitation, after the decoding procedures, the expected signal of each subcarrier may then be stated as:

$$\mathbf{y}[k] = \sqrt{\rho}\mathbf{W}_{\mathrm{BB}}^{H}[k]\mathbf{W}_{\mathrm{RF}}^{H}\mathbf{H}[k]\mathbf{F}_{\mathrm{RF}}\mathbf{F}_{\mathrm{BB}}[k]\mathbf{s} + \mathbf{W}_{\mathrm{BB}}^{H}[k]\mathbf{W}_{\mathrm{RF}}^{H}\mathbf{n}, \tag{3.29}$$

where the subcarrier index $k \in [0, K - 1]$. $\mathbf{H}[k]$: kth sub-carrier frequency domain channel matrix, specified by [20] as.

$$\mathbf{H}[k] = \gamma \sum_{\mathrm{i}=0}^{\mathrm{N_{cl}}-1} \sum_{\mathrm{l}=1}^{\mathrm{N_{ray}}} \alpha_{\mathrm{il}} a_{\mathrm{r}} (\varphi_{\mathrm{il}}^{\mathrm{r}}, \theta_{\mathrm{il}}^{\mathrm{r}}) a_{\mathrm{t}}(\varphi_{\mathrm{il}}^{\mathrm{t}}, \theta_{\mathrm{il}}^{\mathrm{t}})^{\mathrm{H}} \mathrm{e}^{-\mathrm{j}2\pi \mathrm{ik}/\mathrm{K}} \tag{3.30}$$

where the normalization factor is $\sqrt{\frac{N_t N_r}{N_{\mathrm{cl}} N_{\mathrm{ray}}}}$, and K is total number of sub-carriers. In mm-wave MIMO-OFDM systems, the hybrid precoder architecture in [20] can be expressed as:

$$\text{minimize } (\mathbf{F}_{\mathrm{RF}}\mathbf{F}_{\mathrm{BB}}[k]) \quad \sum_{k=0}^{K-1} \left\| \mathbf{F}_{\mathrm{opt}}[k] - \mathbf{F}_{\mathrm{RF}}\mathbf{F}_{\mathrm{BB}}[k] \right\|_{\mathrm{F}}^{2}$$

$$\text{subject to} \quad \begin{cases} \mathbf{F}_{\mathrm{RF}} \in \mathrm{A} \\ \| \mathbf{F}_{\mathrm{RF}}\mathbf{F}_{\mathrm{BB}}[k] \|_{\mathrm{F}}^{2} = N_s \end{cases} \tag{3.31}$$

where optimal digital precoder for kth sub-carrier is $\mathbf{F}_{\mathrm{opt}}[k]$. Although the spectral efficiency is not explicitly maximized, as in the case of narrowband, see [11], [22], the objective is a nice alternative that will allow this problem to be manageable.

Alternating minimization structure may be embraced to resolve problem (3.31). Moreover, since we can eliminate the summation in (3.31), it is possible to update the digital precoder of the entire sub-carrier in a parallel manner, while the digital precoder of every sub-carrier is being optimized. Thus, problem (3.31) still abides by the solutions from (3.7), and (3.28). The next focus is the architectural layout of the analog precoding, and that is the key distinction from narrow-band system. Hence, in OFDM systems, the algorithms of AltMin may be incorporated into hybrid precoding. As regards to the algorithm of MO-AltMin, using manifold optimization principles, as

stated in subsection 3.2, Euclidean gradient of the objective function in (3.31) is first derived and is:

$$\nabla f(\mathrm{x}) = -2\sum_{k=0}^{K-1}\left(\mathbf{F}_{\mathrm{BB}}^{*}[k] \otimes \mathbf{I}_{N_t}\right) \mathrm{x}\left[\mathrm{vec}\left(\mathbf{F}_{\mathrm{opt}}[k]\right) - \left(\mathbf{F}_{\mathrm{BB}}^{T}[k] \otimes \mathbf{I}_{N_t}\right)\mathbf{x}\right]. \quad (3.32)$$

Once Euclidean gradient is determined, the mapped gradient vector and Riemannian gradient can be found on the manifold by using both the projection in (3.13) and the retraction in (3.15). In terms of the algorithm of PE-AltMin, the problem generated for the design of the analog precoder can be seen below, following an identical upper bound and some kind of manipulations implemented in subsection 3.3.

$$\text{minimize } (\mathbf{F}_{\mathrm{RF}}) \quad \sum_{k=0}^{K-1}\left\|\mathbf{F}_{\mathrm{opt}}[k]\mathbf{F}_{\mathrm{DD}}^{H}[k] - \mathbf{F}_{\mathrm{RF}}\right\|_{\mathrm{F}}^{2}$$

$$\text{subject to } \left|(\mathbf{F}_{\mathrm{RF}})_{i,j}\right| = 1, \forall \mathrm{i}, \mathrm{j} \quad (3.33)$$

that has solutions in closed forms,

$$\arg(\mathbf{F}_{\mathrm{RF}}) = \arg\left(\sum_{k=0}^{K-1}\mathbf{F}_{\mathrm{opt}}[k]\mathbf{F}_{\mathrm{DD}}^{H}[k]\right). \quad (3.34)$$

In replacing line (5) with (3.34) within the algorithm of PE-AltMin, such approach allows algorithm of PE-AltMin to be implemented on OFDM system.

Thus, in relations to the analog precoder, solutions in closed form can be achieved as:

$$\arg\left\{(\mathbf{F}_{\mathrm{RF}})_{i,l}\right\} = \arg\left\{\sum_{k=0}^{K-1}\left(\mathbf{F}_{\mathrm{opt}}[k]\right)_{i,:}\left(\mathbf{F}_{\mathrm{DD}}^{H}[k]\right)_{l,:}{}^{H}\right\},$$

$$1 \le i \le N_t,\ l = \left\lceil i\frac{N_{\mathrm{RF}}^{t}}{N_t}\right\rceil \quad (3.35)$$

The above-mentioned solutions reveal that the algorithm of AltMin may be incorporated directly into mm-wave MIMO-OFDM system and simulation results in Chapter 4 of this thesis will demonstrate the effectiveness of the algorithm of AltMin.

Chapter 4

SIMULATION RESULTS

This chapter provides numerical assessments on the efficiency of the algorithms. In practicable mm-Wave MIMO systems, the base-station usually can handle massive number of transmitter antennas compared to the mobile terminals [57]. It is also worthy of note that the wavelength is in millimeter and since half wavelength is the focus of study in this thesis, the dimension of the antennas would also be in millimeter. Hence, the number of transmitted antenna is larger than the received antenna. Therefore, streams of data transmitted from a transmitter with N_t = 144 are sent to the receiver with N_r = 36 antennas, each of them are well set up with USPA. The criteria of the channels could be defined by N_{ray} = 10 rays, N_{cl}= 5 clusters, and every cluster has an average power of $\sigma_{\alpha,i}^2$ = 1. The Laplacian distribution is trailed by azimuth and elevation AoD and AOA with mean angles that are uniformly distributed over [0, 2π) and a 10-degree angular range. The antennas component of USPA is divided by a distance of half wavelength, while on the average all simulations are done at about 1000 channel realizations. In the analog precoder $\mathbf{F}_{\text{RF}}$ early stages, the distributions over [0, 2π) are uniform for all the algorithms of AltMin.

4.1 Evaluation of Spectral Efficiency

The first is to evaluate spectral efficiency from different algorithms when the amount of data streams is equal to the number of RF chains, i.e., $N_{\text{RF}}^t = N_{\text{RF}}^r = N_s$. This situation is the worst because it is not possible to reduce the number of RF chains going by the assumptions of section 3.1.1. As seen in Figure 4.1, the optimal digital

precoder can achieve much higher spectral efficiency than OMP algorithm [11]. On the contrary, the algorithm of MO-AltMin performs almost optimally in the entire SNR range. However, in relation to analog beamforming, algorithms of OMP and MO-AltMin both offers significant performance gains, particularly as SNR is increasing. Essentially, even with RF chains being constrained, MO-AltMin algorithms can become more accurate in approximation to optimal digital precoder as compared to other algorithms.

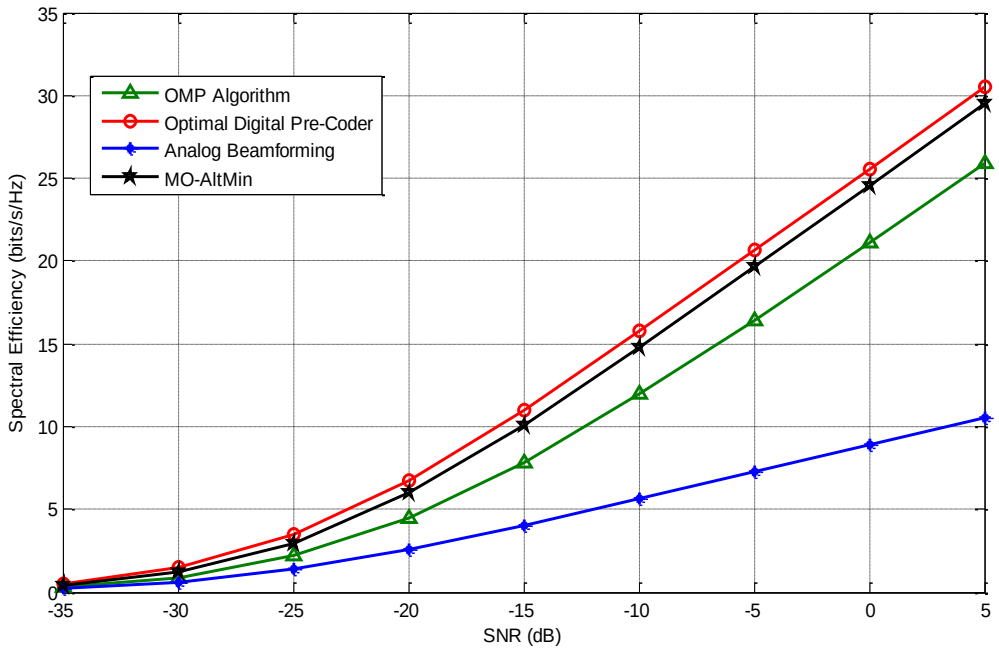

Figure 4.1: Spectral efficiency realized from various precoding algorithms when $N_{\mathrm{RF}}^{t} = N_{\mathrm{RF}}^{r} = N_s = 3$.

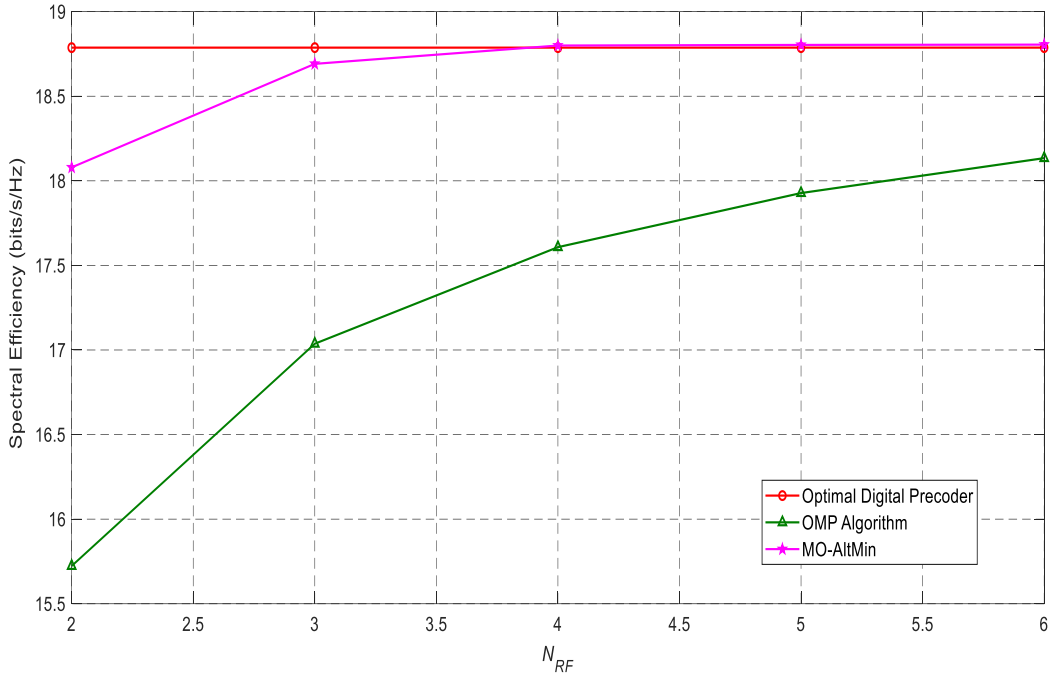

Figure 4.2: Spectral efficiency realized from various precoding algorithms where $N_s = 2$, $N_{\mathrm{RF}}^t = N_{\mathrm{RF}}^r = \mathrm{N_{RF}}$ and SNR = 0 dB.

In [26], it is shown that when $N_{\mathrm{RF}}^t \geq 2N_s$ and $N_{\mathrm{RF}}^r \geq 2N_s$, for the hybrid precoding, a solution in a closed form to the design problem is equivalent to the spectral efficiency realized out of optimal digital precoder. Even though, in this study, the hybrid precoder design is aimed at cases of $N_s \leq N_{\mathrm{RF}}^t < 2N_s$.

Figure 4.2 shows the efficiency of various precoding techniques for several N_{RF}. It can be seen that MO-AltMin algorithm and the optimal digital precoder begins to correspond when $N_{\mathrm{RF}}^t = N_{\mathrm{RF}}^r \geq 4$. This result shows that the algorithm can achieve the optimum spectral efficiency when $N_{\mathrm{RF}}^t \geq 2N_s$ and $N_{\mathrm{RF}}^r \geq 2N_s$, but cannot however be accomplished by OMP algorithm.

4.2 Low-Complexity Design

As stated in Section 3.3, the design of the algorithm of PE-AltMin requires two transitional phases, simply put, using orthogonal columns to construct digital precoder

as well as employing the use of upper limit to replace the objective function. The impact of more restrictions placed on digital precoder is tested through making sure amount of RF chains as well as data streams are equivalent, that is to say, strengthen the bond such that the effect of the second step is removed.

Figure 4.3 shows the spectral efficiency obtained from the algorithm of MO-AltMin as well as that of PE-AltMin for the transmission of data streams 2, 4 and 8. It can be seen that PE-AltMin low-complexity curves are almost the same as the algorithm of MO-AltMin. This discovery thus reveals that the effect on the spectral efficiency is minimal because of the orthogonal arrangement of the digital precoder, and that explains the reasoning in Section 3.3 of the digital precoder model.

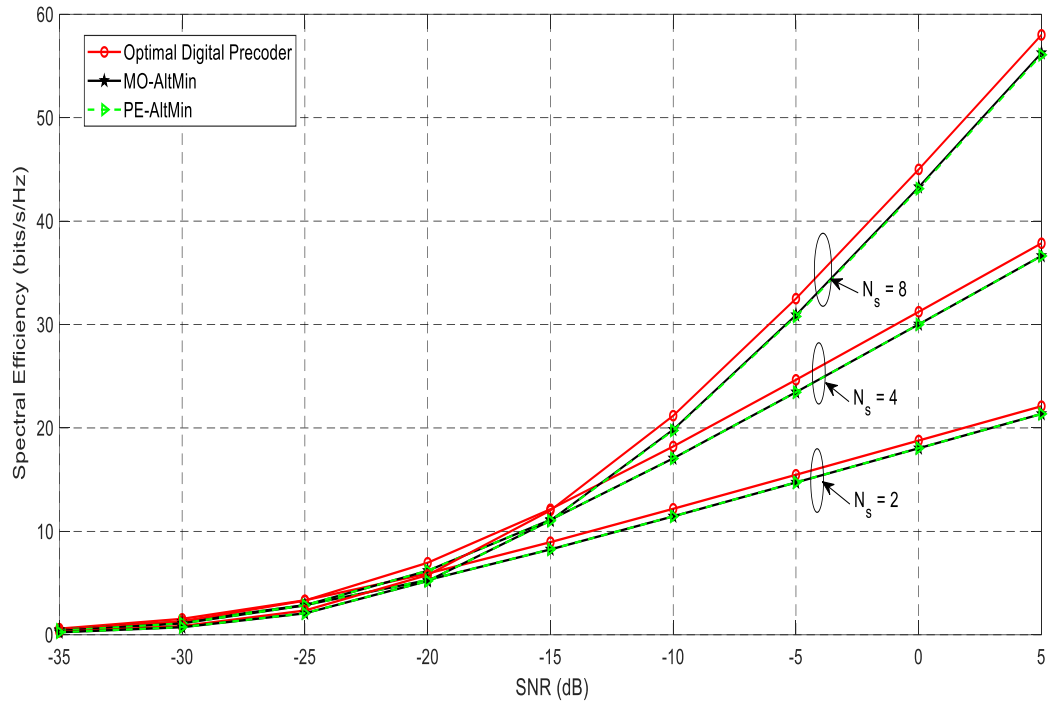

Figure 4.3: Spectral efficiency realized from the algorithm of MO-AltMin and PE-AltMin where $N_{\mathrm{RF}}^{t} = N_{RF}^{r} = N_{\mathrm{RF}} = N_{s}$.

Figure 4.3 also reveals that the algorithm of MO-AltMin having tremendous complexities could also be achieved by embracing PE-AltMin algorithm with low-complexity where $N_{\mathrm{RF}} = N_{\mathrm{s}}$ is used. More so, the algorithm of PE-AltMin sets out to be an outstanding prospect for the design of the hybrid precoder under the same system setting, thereby, achieving great results as well as lower complexity.

Furthermore, the effect of the amount of RF chains is investigated. Figure 4.4 gives the comparison of different algorithm when 6 data streams are transmitted ($N_{\mathrm{s}} = 6$). While the right approach is thoroughly formulated for $N_{\mathrm{RF}}^{t} \geq 2N_s$ case, $N_{\mathrm{RF}}^{t} = N_{\mathrm{RF}}^{r} = N_{\mathrm{RF}} \in [6, 11]$ is examined here. From Figure 4.4, it can be noted that there is a slight difference in the algorithm of PE-AltMin and the algorithm of MO-AltMin. For the reason that, in contrast to the low-complexity algorithm to try to minimize original objective function, it tries to minimize the upper bound.

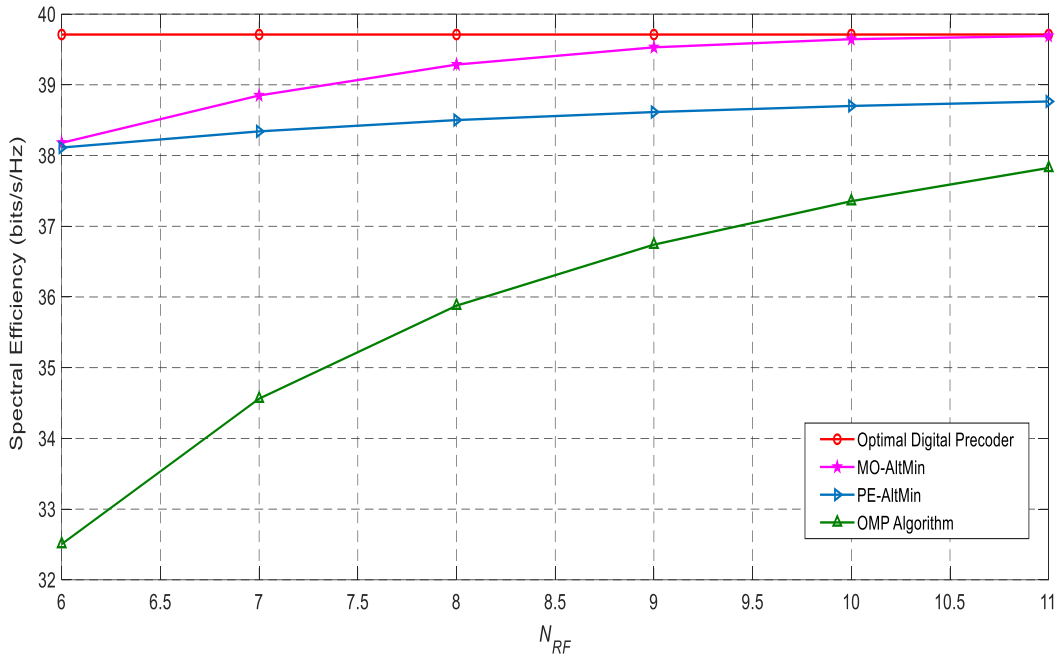

Figure 4.4: Spectral efficiency realized from various precoding algorithms where $N_s = 6$, $N_{\mathrm{RF}}^{t} = N_{\mathrm{RF}}^{r} = N_{\mathrm{RF}}$ and SNR = 0 dB.

As stated in section 3.3, when $N_{\mathrm{RF}} = N_s$, the upper bound becomes tight but when N_{RF} increases, it loosens, and that establishes the difference between the algorithms of MO-AltMin and PE-AltMin. Nonetheless, the algorithm of PE-AltMin's spectral efficiency is much greater to that of OMP algorithm, particularly in a case where the number of RF chain is quite small. AltMin algorithms demonstrate that the algorithm of MO-AltMin almost coincide with the digital precoder once the amount of data streams is like the number of RF chains, that could not be seen in OMP algorithm.

4.3 Hybrid Precoding for mm-Wave MIMO-OFDM Systems

This section discusses the effectiveness of the algorithm of AltMin for mm-Wave MIMO-OFDM systems. The number of subcarriers is assumed to be K = 128. Figure 4.5 illustrates the spectral efficiency realized from the algorithms of MO-AltMin and PE-AltMin as well as how it compares to that of OMP-based algorithm.

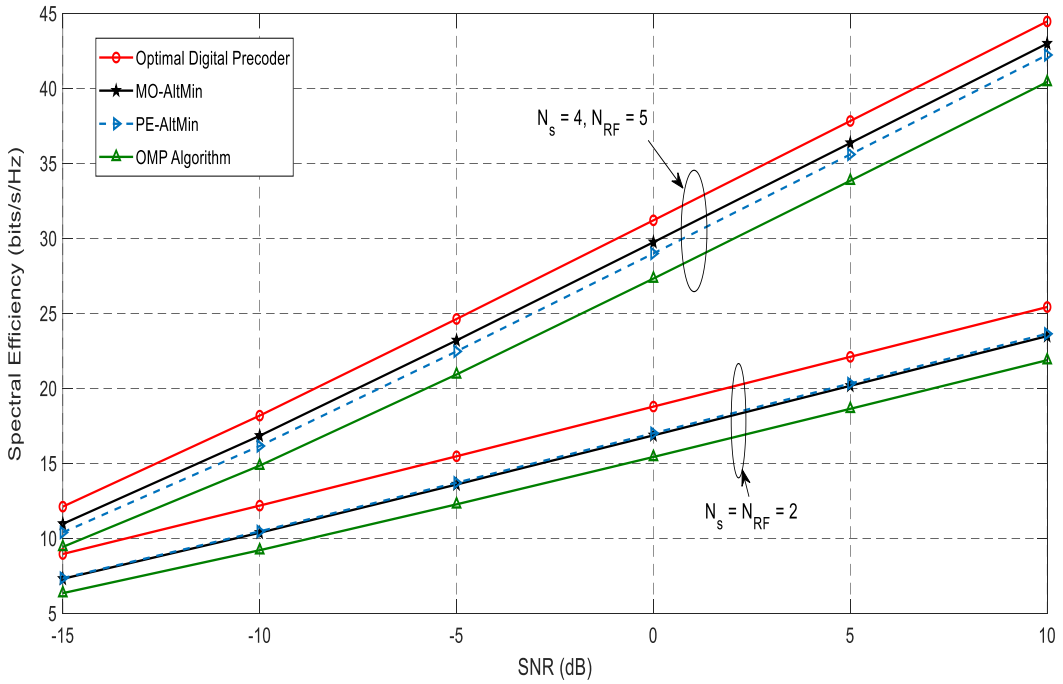

Figure 4.5: Spectral efficiency obtained from various precoding algorithms in mm-Wave MIMO-OFDM systems where $N_{\mathrm{RF}}^{t} = N_{\mathrm{RF}}^{r} = N_{\mathrm{RF}}$.

It became apparent that subject to various system factors, the algorithm of MO-AltMin still has the greatest spectral efficiency. Similarly, to the observation made in Figure 4.4, when RF chains is large, the algorithm of MO-AltMin rapidly achieves maximal efficiency for the digital precoder. It is also important to bear in mind that when the amount of data streams is equal to the number of RF chains, the low-complexity algorithm of PE-AltMin could actually accomplish similar spectral efficiency to the algorithm of MO-AltMin. However, in narrowbands that is precisely an identical case, that particularly illustrates that in mm-Wave OFDM systems, a minimal effect on spectral efficiency follows when the digital precoder is subjected to additional orthogonality restriction. It can also be seen in Figure 4.5 that in mm-Wave OFDM system, the algorithm of PE-AltMin performs exceedingly better compare to the algorithm of OMP-based. Hence, this reveals that the algorithm of PE-AltMin can be used as an excellent choice both in broadband OFDM systems and narrowband for hybrid precoding based low-complexity when the transceivers are only reached by short RF chains.

Chapter 5

CONCLUSION AND FUTURE WORK

In this thesis, an extensive analysis of hybrid precoding that involves mm-Wave MIMO system using an alternating minimization algorithm was explained. I have also explained how technology went from the time before 1G to a time where the mobile market will experience a fresh mobile revolution with 5G. A revolution that will require much higher internet speed where networks will have the best trade-offs for trillions of connecting gadgets in terms of speed, latency, energy efficiency and price. To lay a bit more emphasis on latency rate, let envision a world where a vehicle reacts 250 times quicker than human because its reaction time is 1ms. This is all because of the extremely low latency rate that 5G offers, from 200 ms in 4G to 1ms in 5G. I have also explained that without the advent of mm-Wave technology with a frequency band between 30 GHz and 300 GHz, no one would even dare think of 5G technology. In spite of its attenuation losses and free space losses, I have discussed in this thesis that it is still the utmost operational solution to the current outpour in wireless internet usage. Furthermore, I have also explained the importance of MIMO technology. MIMO makes it possible to increase the efficiency of the wireless connection between the transmitter and the receiver. Its rich multi-path environment allows the generation of multiple orthogonal channels between the transmitter and the receiver. MIMO helps to improve power efficiency as well as increase capacity gain or combat signal fading. In addition, hybrid precoding was also discussed. A technique that makes the possibility of clusters of information to be concurrently transmitted to multiple users without any

interruption. What's more, in this thesis, using the principle of alternating minimization, a ground-breaking design methodology for hybrid precoding in mm-Wave MIMO systems was discussed. Effective algorithms for hybrid precoding have been discussed, and findings from simulations has aided in revealing useful insights that if the amount of RF chains is marginally greater than the amount of streams of data, hybrid precoders may reach an achievement level that can be compared to fully digital precoder. Taking into account the rising expense and energy usage, there really should not be any reason to boost the amount of RF chains much farther. Simulation results in relations to spectral efficiency have also shown that MO-AltMin algorithm performs satisfactorily in contrast to a number of existing algorithms. Finally, in mm-Wave MIMO systems, simulation outcomes have undeniably shown the reliability of alternating minimization in the design of hybrid precoders.

For future work, it would be fascinating to see how alternating minimization approach can be extended to other design issues of hybrid precoder and how the hybrid precoder concept can be integrated with reviews and channel development. Further research will also involve a more resounding convergence review and a refinement of the algorithm that was conceptualized.

REFERENCES

[1] Ericsson mobility report: June 2016," Available at https://www.ericsson.com/res/docs/2016/ericsson-mobility-report-2016.pdf.

[2] Qualcomm, “The evolution of mobile technologies," Tech. Rep., 2014

[3] Torkildson, E., Madhow, U., & Rodwell, M. (2011). Indoor millimeter wave MIMO: Feasibility and performance. *IEEE Transactions on Wireless Communications*, *10*(12), 4150-4160.

[4] Rappaport, T. S., Heath Jr, R. W., Daniels, R. C., & Murdock, J. N. (2014). *Millimeter wave wireless communications*. Pearson Education.

[5] Hoydis, J., Ten Brink, S., & Debbah, M. (2013). Massive MIMO in the UL/DL of cellular networks: How many antennas do we need?. *IEEE Journal on selected Areas in Communications*, *31*(2), 160-171.

[6] Li, C., Zhang, J., & Letaief, K. B. (2014). Throughput and energy efficiency analysis of small cell networks with multi-antenna base stations. *IEEE Transactions on Wireless Communications*, *13*(5), 2505-2517.

[7] Bartoli, G., Fantacci, R., Letaief, K., Marabissi, D., Privitera, N., Pucci, M., & Zhang, J. (2014). Beamforming for small cell deployment in LTE-advanced and beyond. *IEEE Wireless Communications*, *21*(2), 50-56.

[8] Doppler, K., Rinne, M., Wijting, C., Ribeiro, C. B., & Hugl, K. (2009). Device-to-device communication as an underlay to LTE-advanced networks. *IEEE Communications Magazine*, *47*(12).

[9] Shi, Y., Zhang, J., Letaief, K. B., Bai, B., & Chen, W. (2015). Large-scale convex optimization for ultra-dense Cloud-RAN. *IEEE Wireless Communications*, *22*(3), 84-91.

[10] Shi, Y., Zhang, J., & Letaief, K. B. (2014). Group sparse beamforming for green cloud-RAN. *IEEE Transactions on Wireless Communications*, *13*(5), 2809-2823.

[11] El Ayach, O., Rajagopal, S., Abu-Surra, S., Pi, Z., & Heath, R. W. (2014). Spatially sparse precoding in millimeter wave MIMO systems. *IEEE transactions on wireless communications*, *13*(3), 1499-1513.

[12] Akdeniz, M. R., Liu, Y., Samimi, M. K., Sun, S., Rangan, S., Rappaport, T. S., & Erkip, E. (2014). Millimeter wave channel modeling and cellular capacity evaluation. *IEEE journal on selected areas in communications*, *32*(6), 1164-1179.

[13] Zhang, E., & Huang, C. (2014, September). On achieving optimal rate of digital precoder by RF-baseband co-design for MIMO systems. In *Vehicular Technology Conference (VTC Fall), 2014 IEEE 80th* (pp. 1-5). IEEE.

[14] Roh, W., Seol, J. Y., Park, J., Lee, B., Lee, J., Kim, Y., ... & Aryanfar, F. (2014). Millimeter-wave beamforming as an enabling technology for 5G cellular

communications: Theoretical feasibility and prototype results. *IEEE communications magazine*, *52*(2), 106-113.

[15] Sun, S., Rappaport, T. S., Heath, R. W., Nix, A., & Rangan, S. (2014). MIMO for millimeter-wave wireless communications: beamforming, spatial multiplexing, or both?. *IEEE Communications Magazine*, *52*(12), 110-121.

[16] Alkhateeb, A., El Ayach, O., Leus, G., & Heath, R. W. (2014). Channel estimation and hybrid precoding for millimeter wave cellular systems. *IEEE Journal of Selected Topics in Signal Processing*, *8*(5), 831-846.

[17] Wang, P., Li, Y., Song, L., & Vucetic, B. (2015). Multi-gigabit millimeter wave wireless communications for 5G: From fixed access to cellular networks. *IEEE Communications Magazine*, *53*(1), 168-178.

[18] Rangan, S., Rappaport, T. S., & Erkip, E. (2014). Millimeter-wave cellular wireless networks: Potentials and challenges. *Proceedings of the IEEE*, *102*(3), 366-385.

[19] Lee, Y. Y., Wang, C. H., & Huang, Y. H. (2015). A hybrid RF/baseband precoding processor based on parallel-index-selection matrix-inversion-bypass simultaneous orthogonal matching pursuit for millimeter wave MIMO systems. *IEEE Transactions on Signal Processing*, *63*(2), 305-317.

[20] Lee, J., & Lee, Y. H. (2014, June). AF relaying for millimeter wave communication systems with hybrid RF/baseband MIMO processing. In *Communications (ICC), 2014 IEEE International Conference on* (pp. 5838-5842). IEEE.

[21] Kim, M., & Lee, Y. H. (2015). MSE-based hybrid RF/baseband processing for millimeter-wave communication systems in MIMO interference channels. *IEEE Transactions on Vehicular Technology*, *64*(6), 2714-2720.

[22] Brady, J., Behdad, N., & Sayeed, A. M. (2013). Beamspace MIMO for millimeter-wave communications: System architecture, modeling, analysis, and measurements. *IEEE Transactions on Antennas and Propagation*, *61*(7), 3814-3827.

[23] Rusu, C., Méndez-Rial, R., González-Prelcicy, N., & Heath, R. W. (2015, June). Low complexity hybrid sparse precoding and combining in millimeter wave MIMO systems. In *Communications (ICC), 2015 IEEE International Conference on* (pp. 1340-1345). IEEE.

[24] Singh, J., & Ramakrishna, S. (2015). On the feasibility of codebook-based beamforming in millimeter wave systems with multiple antenna arrays. *IEEE Transactions on Wireless Communications*, *14*(5), 2670-2683.

[25] Kim, C., Kim, T., & Seol, J. Y. (2013, December). Multi-beam transmission diversity with hybrid beamforming for MIMO-OFDM systems. In *Globecom Workshops (GC Wkshps), 2013 IEEE* (pp. 61-65). IEEE.

[26] Dai, L., Gao, X., Quan, J., Han, S., & Chih-Lin, I. (2015, June). Near-optimal hybrid analog and digital precoding for downlink mmWave massive MIMO systems. In *Communications (ICC), 2015 IEEE International Conference on* (pp. 1334-1339). IEEE.

[27] Han, S., Chih-Lin, I., Xu, Z., & Rowell, C. (2015). Large-scale antenna systems with hybrid analog and digital beamforming for millimeter wave 5G. *IEEE Communications Magazine*, *53*(1), 186-194.

[28] Love, D. J., & Heath, R. W. (2005). Limited feedback unitary precoding for spatial multiplexing systems. *IEEE Transactions on Information theory*, *51*(8), 2967-2976.

[29] Jain, P., Netrapalli, P., & Sanghavi, S. (2013, June). Low-rank matrix completion using alternating minimization. In *Proceedings of the forty-fifth annual ACM symposium on Theory of computing* (pp. 665-674). ACM.

[30] Netrapalli, P., Jain, P., & Sanghavi, S. (2013). Phase retrieval using alternating minimization. In *Advances in Neural Information Processing Systems* (pp. 2796-2804).

[31] Wang, Y., Yang, J., Yin, W., & Zhang, Y. (2008). A new alternating minimization algorithm for total variation image reconstruction. *SIAM Journal on Imaging Sciences*, *1*(3), 248-272.

[32] Chan, T. F., & Wong, C. K. (2000). Convergence of the alternating minimization algorithm for blind deconvolution. *Linear Algebra and its Applications*, *316*(1-3), 259-285.

[33] Kim, H., & Park, H. (2008). Nonnegative matrix factorization based on alternating nonnegativity constrained least squares and active set method. *SIAM journal on matrix analysis and applications*, *30*(2), 713-730.

[34] Zhang, X., Molisch, A. F., & Kung, S. Y. (2005). Variable-phase-shift-based RF-baseband codesign for MIMO antenna selection. *IEEE Transactions on Signal Processing*, *53*(11), 4091-4103.

[35] Absil, P. A., Mahony, R., & Sepulchre, R. (2009). *Optimization algorithms on matrix manifolds*. Princeton University Press.

[36] Lee, J. M. (2013). Smooth Manifolds. In *Introduction to Smooth Manifolds* (pp. 1-31). Springer New York.

[37] Shi, Y., Zhang, J., & Letaief, K. B. (2015, June). Low-rank matrix completion via Riemannian pursuit for topological interference management. In *Information Theory (ISIT), 2015 IEEE International Symposium on* (pp. 1831-1835). IEEE.

[38] Hjørungnes, A. (2011). *Complex-valued matrix derivatives: with applications in signal processing and communications*. Cambridge University Press.

[39] Boumal, N., Mishra, B., Absil, P. A., & Sepulchre, R. (2014). Manopt, a matlab toolbox for optimization on manifolds. *Journal of Machine Learning Research*, *15*(1), 1455-1459.

[40] Patrascu, A., & Necoara, I. (2015). Efficient random coordinate descent algorithms for large-scale structured nonconvex optimization. *Journal of Global Optimization, 61*(1), 19-46.

[41] Luo, Z. Q., Ma, W. K., So, A. M. C., Ye, Y., & Zhang, S. (2010). Semidefinite relaxation of quadratic optimization problems. *IEEE Signal Processing Magazine, 27*(3), 20-34.

[42] Boyd, S., & Vandenberghe, L. (2004). *Convex optimization*. Cambridge university press.

[43] Vashist, V. (2015). 5th generation technology. *International Journal Of Advanced Technology In Engineering and Science*.

[44] Tuan, N. (2017). Small cell networks and the evolution of 5G. *Qorvo,* 24 September 2019 < https://www.qorvo.com/design-hub/blog/small-cell-networks-and-the-evolution-of-5g >

[45] Gary, H. (2019). 5G needs more memory to compute. *EE Times,* 24 September 2019 < https://www.eetimes.com/document.asp?doc_id=1334512&image_number=1>

[46] Nagapushpa, K. P., & Chitra, K. N. (2017). Studying Applicability Feasibility of OFDM in Upcoming 5G Network. (*IJACSA) International Journal of Advanced Computer Science and Applications, 8*(1), 216-220.

[47] Cisco, V. (2010). Cisco Visual Networking Index: Forecast and Methodology 2009–2014.

[48] wave Propagation, M. (1997). Spectrum Management Implications. –FCC, Office of Eng. and Tech. *Bulletin*, (70).

[49] MIMO Systen. *Elprocus*, 17 October 2019 < https://www.elprocus.com/mimo-multiple-input-multiple-output-technology/>

[50] Alamouti, S. M. (1998). A simple transmit diversity technique for wireless communications. *1998*.

[51] Tarokh, V., Jafarkhani, H., & Calderbank, A. R. (1999). Space-time block codes from orthogonal designs. *IEEE Transactions on Information theory*, *45*(5), 1456-1467.

[52] Tarokh, V., Seshadri, N., & Calderbank, A. R. (1998). Space-time codes for high data rate wireless communication: Performance criterion and code construction. *IEEE transactions on information theory*, *44*(2), 744-765.

[53] Wolniansky, P. W., Foschini, G. J., Golden, G. D., & Valenzuela, R. A. (1998, October). V-BLAST: An architecture for realizing very high data rates over the rich-scattering wireless channel. In *1998 URSI international symposium on signals, systems, and electronics. Conference proceedings (Cat. No. 98EX167)* (pp. 295-300). IEEE.

[54] Ha, J., Mody, A. N., Sung, J. H., Barry, J. R., McLaughlin, S. W., & Stüber, G. L. (2002). LDPC coded OFDM with Alamouti/SVD diversity technique. *Wireless Personal Communications*, *23*(1), 183-194.

[55] Anderson, C. R., & Rappaport, T. S. (2004). In-building wideband partition loss measurements at 2.5 and 60 GHz. *IEEE transactions on wireless communications*, *3*(3), 922-928.

[56] Chen, C. H., Tsai, C. R., Liu, Y. H., Hung, W. L., & Wu, A. Y. (2016). Compressive sensing (CS) assisted low-complexity beamspace hybrid precoding for millimeter-wave MIMO systems. *IEEE Transactions on Signal Processing*, *65*(6), 1412-1424.

[57] Liu, X., Li, X., Cao, S., Deng, Q., Ran, R., Nguyen, K., & Tingrui, P. (2019). Hybrid precoding for massive mmWave MIMO systems. *IEEE Access*, *7*, 33577-33586.